Physica D 428 (2021) 133051

Contents lists available at ScienceDirect

Physica D

journal homepage: www.elsevier.com/locate/physd

On solitary-wave solutions of Boussinesq/Boussinesq systems for internal waves

Vassilios A. Dougalis [a,b], Angel Durán [c,*], Leetha Saridaki [a,b]

[a] Mathematics Department, University of Athens, 15784 Zographou, Greece
[b] Institute of Applied & Computational Mathematics, FO.R.T.H., 71110 Heraklion, Greece
[c] Applied Mathematics Department, University of Valladolid, 47011 Valladolid, Spain

ARTICLE INFO

Article history:
Received 31 March 2021
Received in revised form 17 September 2021
Accepted 18 September 2021
Available online 29 September 2021
Communicated by T. Wanner

Keywords:
Internal waves
Boussinesq/Boussinesq systems
Solitary waves
Spectral methods

ABSTRACT

In this paper we consider a three-parameter system of Boussinesq/Boussinesq type, modeling the propagation of internal waves. Some theoretical and numerical properties of the systems were previously analyzed by the authors. As a second part of the study, the present paper is concerned with the analysis of existence and the numerical simulation of some issues of the dynamics of solitary-wave solutions. Standard theories are used to derive several results of existence of classical and generalized solitary waves, depending on the parameters of the models. A numerical procedure based on a Fourier collocation approximation for the ode system of the solitary wave profiles with periodic boundary conditions, and on the iterative solution of the resulting fixed-point equations with the Petviashvili scheme combined with vector extrapolation techniques, is used to generate numerically approximations of solitary waves. These are an essential part of a computational study of the dynamics of the solitary waves, both classical and generalized. Using a full discretization based on spectral approximation in space of the corresponding periodic initial-value problem for the systems, and a fourth-order Runge–Kutta method of composition type as time integrator, we explore the evolution of small and large perturbations of the computed solitary-wave profiles, and we study computationally the collisions of solitary waves as well as the resolution of initial data into trains of solitary waves.

1. Introduction

In a previous paper, [1], see also [2], the authors considered the three-parameter family of Boussinesq/Boussinesq (B/B) systems

$$\begin{aligned}(1-b\partial_{xx})\zeta_t+\frac{1}{\gamma+\delta}\partial_x v_\beta+\left(\frac{\delta^2-\gamma}{(\delta+\gamma)^2}\right)\partial_x\left(\zeta v_\beta\right)\\ +a\partial_{xxx}v_\beta=0\\ (1-d\partial_{xx})(v_\beta)_t+(1-\gamma)\partial_x\zeta+\left(\frac{\delta^2-\gamma}{2(\delta+\gamma)^2}\right)\partial_x v_\beta^2\\ +(1-\gamma)c\partial_{xxx}\zeta=0,\end{aligned}\tag{1.1}$$

derived by Bona, Lannes and Saut, [3], as a one-dimensional approximation to the two-dimensional Euler equations for internal wave propagation along the interface of a two-layer system of fluids, with a rigid-lid condition for the upper layer while the lower layer is bounded below by a horizontal, impermeable bottom. In (1.1), wherein the variables are nondimensional and unscaled, $x\in\mathbb{R}$, $t\geqslant 0$, $\zeta=\zeta(x,t)$ denotes the interfacial deviation and $v_\beta=(1-\beta\partial_{xx})^{-1}u$, with $\beta\geqslant 0$ a modeling parameter, and where $u=u(x,t)$ is a velocity variable. The parameter $\gamma\in(0,1)$ stands for the density ratio between upper and lower layers. The constants a,b,c,d are of the form

$$\begin{aligned}a=\frac{(1-\alpha_1)(1+\gamma\delta)-3\delta\beta(\delta+\gamma)}{3\delta(\gamma+\delta)^2},\quad b=\alpha_1\frac{1+\gamma\delta}{3\delta(\gamma+\delta)},\\ c=\beta\alpha_2,\quad d=\beta(1-\alpha_2).\end{aligned}\tag{1.2}$$

where δ denotes the depth ratio between upper and lower layers and $\alpha_1\geqslant 0$ and $\alpha_2\leqslant 1$ are modeling parameters. From (1.2) we have the relation

$$(\delta+\gamma)a+b+c+d=S(\gamma,\delta),\quad S(\gamma,\delta):=\frac{1+\gamma\delta}{3\delta(\gamma+\delta)}.\tag{1.3}$$

The physical regime of validity of (1.1) as approximation to the Euler system and under which it was derived in [3] (see also [4]) is of Boussinesq type in both fluid domains. This means $\delta\approx 1$, and that the dispersive and nonlinear effects are assumed to be small and of comparable size. The case of surface wave propagation, derived and analyzed in [5,6], corresponds to taking $\gamma=0,\delta=1$ in (1.1). In addition, the derivation of (1.1) in [3] assumes that surface tension effects are negligible. This physical

* Corresponding author.
E-mail addresses: doug@math.uoa.gr (V.A. Dougalis), angeldm@uva.es (A. Durán), leetha.saridaki@gmail.com (L. Saridaki).

https://doi.org/10.1016/j.physd.2021.133051
0167-2789/

assumption is mathematically expressed in the condition (1.3) (which is analogous to the formula (1.8) in [5] for the case of surface waves) and establishes a relation among a, b, c and d. Thus, once the physical parameters γ and δ are fixed, system (1.1), under (1.3), can be viewed as dependent on three of the four parameters a, b, c, d or, equivalently, using (1.2), on $\alpha_1, \alpha_2, \beta$, that we treat as modeling parameters.

The present paper continues a study initiated in [1] (for an extended version of both papers see [2]), where the authors discussed several theoretical and numerical issues for (1.1). A summary of the results of [1] is presently given. We first reviewed, in terms of the parameters a, b, c, d, well-posedness properties of the initial-value problem (ivp) for (1.1) using the results of [5,6] for the case of surface wave propagation. It was shown that in the admissible case

(H1) $a, c \leqslant 0, b, d \geqslant 0$,

the ivp for (1.1) is linearly well-posed in suitable Sobolev spaces for ζ and u. Concerning local in time well-posedness of the full nonlinear systems (meaning existence, uniqueness and regularity locally in time of solutions), the application of the theory developed in [6] leads to seven cases of well-posed systems in the indicated pairs of Sobolev spaces as follows:

- Case (i): $b, d > 0, a = c = 0$ ($H^s \times H^s, s \geqslant 0$).
- Case (ii): $b, d > 0, a, c < 0$ ($H^s \times H^s, s \geqslant 0$).
- Case (iii): $b = 0, d > 0, a, c < 0$ ($H^s \times H^{s+3}, s \geqslant 1$).
- Case (iv): $b = 0, d > 0, a = c = 0$, or $b > 0, d = 0, a = c = 0$ ($H^s \times H^{s+1}, s \geqslant 1$; conditional global existence).
- Case (v): $b, d > 0, a = 0, c < 0$ or $b, d > 0, a < 0, c = 0$ ($H^{s+1} \times H^s, s \geqslant 0$; conditional global existence).
- Case (vi): $b = 0, d > 0, a < 0, c = 0$ ($H^s \times H^{s+2}, s \geqslant 1$).
- Case (vii): $b > 0, d = 0, a < 0, c = 0$ or $b = 0, d > 0, a = 0, c < 0$ ($H^s \times H^s, s \geqslant 2$),

where for real s, $H^s = H^s(\mathbb{R})$ denotes the L^2-based Sobolev space over $\mathbb{R}$. (See [7] for further regularity results for some of these systems.) In addition, the system (1.1) has a Hamiltonian structure when $b = d$, as in the surface wave case. It is worth mentioning that since the case of surface waves is a limiting case of (1.1), it is possible to apply recent results on long time existence for the initial-value problem of the system for surface waves, as e. g. in [8–10], and on the asymptotic behavior of solutions, [11,12], to study such issues in the internal-wave case.

Another contribution of [1] concerns the analysis of numerical approximations to (1.1). The corresponding periodic ivp was discretized in space by the spectral Fourier–Galerkin method and L^2 error estimates for the resulting semidiscretization were derived for each case (i)–(vii) of nonlinearly well posed systems. We also introduced a full discretization of the periodic ivp for (1.1) by integrating numerically in time the spectral semidiscrete systems with a fourth-order Runge–Kutta (RK)-composition method based on the implicit midpoint rule, [13–15]. The resulting fully discrete scheme was checked for accuracy, stability, and performance, in [1] by means of numerical experiments.

The present paper continues the analysis of the systems (1.1) by focusing on their solitary-wave solutions. More specifically, we make a complete study of solitary waves of the B/B systems of physical interest, consisting of:

- Theoretical results on existence of classical and generalized solitary waves, depending on the choice of the parameters a, b, c, d of the system and on the speed of the wave.
- A numerical study of generation and dynamics of these solitary waves, which may shed some light on their stability and role on the evolution of general solutions of (1.1).

All this will be developed according to the following plan of the paper. In Section 2 we consider the existence and numerical approximation of such solitary-wave solutions. We apply several techniques for proving existence of solitary waves, namely Normal Form Theory, [16,17], valid for solitary-wave speeds close to the limiting value $c_{\gamma,\delta} = \sqrt{(1-\gamma)/(\delta+\gamma)}$, and Toland's theory, [18], Concentration–Compactness theory, [19], and Positive Operator theory, [20], that predict existence of solitary waves also at larger speeds (relative to $c_{\gamma,\delta}$). We construct in several cases of interest classical and generalized solitary-wave profiles by solving numerically the second-order nonlinear ordinary differential equation (ode) systems satisfied by the solitary waves. The ode systems are discretized by a spectral method and the resulting nonlinear systems of algebraic equations are numerically solved by the iterative Petviashvili scheme, [21,22], accelerated by the Minimal Polynomial extrapolation (MPE) algorithm, [23].

In Section 3 we present a computational study of several issues associated with the stability and the dynamics of classical and generalized solitary waves of B/B systems. We note that a computational study of solitary waves has been carried out in [24] by a spectral-RK scheme, among other, for a B/B system resembling those in the class (vi); classical solitary waves are constructed and their overtaking and head-on collisions are simulated. In [25] the author used a Crank–Nicolson finite difference-relaxation scheme in order to compare the evolution of solutions of B/B systems (for internal waves with free upper surface) with that of the solutions of their associated KdV one-way approximations. In Section 3 of the paper at hand, the ode ivp's resulting from the spectral semidiscretizations of the ivp's for some of the B/B systems are discretized in time by the three-stage, fourth-order accurate diagonally implicit RK method of composition type analyzed in [1] for the case of the KdV equation. With this fully discrete method in hand we study computationally the temporal evolutions emanating from small and larger perturbations of initial classical and generalized solitary waves. We also investigate overtaking and head-on collisions of solitary waves and the resolution of initial profiles into sequences of solitary waves. (For more experiments, see the extended version [2].) We close the paper with a section of concluding remarks.

2. Solitary waves

This section is focused on the existence and numerical generation of solitary-wave solutions of the B/B systems (1.1). We first review the application of several theories of existence and then we illustrate the corresponding results with some examples of numerical generation of the profiles.

2.1. Some existence results

Solitary-wave solutions of (1.1) are of the form $\zeta = \zeta(X), u = u(X)$ where $X = x - c_s t, c_s \neq 0$, and ζ, u satisfy

$$\partial_x \begin{pmatrix} c_s(1-b\partial_{xx}) & -\frac{1}{\delta+\gamma} - a\partial_{xx} \\ -(1-\gamma)(1+c\partial_{xx}) & c_s(1-d\partial_{xx}) \end{pmatrix} \begin{pmatrix} \zeta \\ v_\beta \end{pmatrix} = \varkappa_{\gamma,\delta}\partial_x \begin{pmatrix} \zeta v_\beta \\ \frac{v_\beta^2}{2} \end{pmatrix},$$

where $\varkappa_{\gamma,\delta} = \frac{\delta^2-\gamma}{(\delta+\gamma)^2}$. Classical Solitary Waves (CSW), for which $\zeta, u \to 0$ as $|X| \to \infty$, will be solutions of

$$\begin{pmatrix} c_s(1-b\partial_{xx}) & -\frac{1}{\delta+\gamma} - a\partial_{xx} \\ -(1-\gamma)(1+c\partial_{xx}) & c_s(1-d\partial_{xx}) \end{pmatrix} \begin{pmatrix} \zeta \\ v_\beta \end{pmatrix} = \varkappa_{\gamma,\delta} \begin{pmatrix} \zeta v_\beta \\ \frac{v_\beta^2}{2} \end{pmatrix}. \quad (2.1)$$

In addition, there exist Generalized Solitary Waves (GSW), which satisfy (2.1) but are not CSW's.

2.1.1. Existence via linearization

In the case of small deviations of c_s from the speed of sound the existence of solitary waves can be studied in a similar way to analogous studies in [26,27] by using Bifurcation theory, [16,17]. For the case of (2.1), we define $c_{\gamma,\delta}$ to be the speed of sound corresponding to (1.1), i. e. as

$$c_{\gamma,\delta} = \sqrt{\frac{1-\gamma}{\delta+\gamma}}, \tag{2.2}$$

Note that if (c_s, ζ, v_β) is a solution of (2.1), then $(-c_s, \zeta, -v_\beta)$ is also a solution (with the same profile but opposite speed). Thus we can assume $c_s > 0$ and define the parameter

$$\widetilde{\mu} := \frac{c_s}{c_{\gamma,\delta}} - 1, \tag{2.3}$$

so that $c_s = \widetilde{\mu} c_{\gamma,\delta} + 1$. The parameter $\widetilde{\mu}$ given by (2.3) is analogous to the parameter μ used in [28] to study, via the Normal Form Theory (NFT), the existence of solitary waves for free surface wave propagation on an inviscid fluid layer under gravity and surface tension effects. In terms of the variables ζ, v_β, (2.1) can be rewritten as a first-order system, depending on $\widetilde{\mu}$, for $U = (U_1, U_2, U_3, U_4)^T := (\zeta, \zeta', v_\beta, v_\beta')^T$, namely as

$$U' = V(U, \widetilde{\mu}) := L(\widetilde{\mu})U + R(U, \widetilde{\mu}), \tag{2.4}$$

$$L(\widetilde{\mu}) = \begin{pmatrix} 0 & 1 & 0 & 0 \\ \frac{dc_s^2 + a(1-\gamma)}{D} & 0 & -\frac{c_s}{D}\left(a + \frac{d}{\delta+\gamma}\right) & 0 \\ 0 & 0 & 0 & 1 \\ -\frac{(1-\gamma)c_s(b+c)}{D} & 0 & \frac{1}{D}\left(bc_s^2 + \frac{c(1-\gamma)}{\delta+\gamma}\right) & 0 \end{pmatrix},$$

$$R(U, \widetilde{\mu}) = \begin{pmatrix} 0 \\ \frac{1}{D}\frac{\delta^2-\gamma}{(\delta+\gamma)^2}\left(-dc_s U_1 U_3 + \frac{a}{2}U_3^2\right) \\ 0 \\ \frac{1}{D}\frac{\delta^2-\gamma}{(\delta+\gamma)^2}\left(-c(1-\gamma)U_1 U_3 - \frac{bc_s}{2}U_3^2\right) \end{pmatrix},$$

$$D = bdc_s^2 - (1-\gamma)ac = bdc_s^2 - \frac{ac}{\varkappa_1}c_{\gamma,\delta}^2, \ \varkappa_1 := \frac{1}{\delta+\gamma}. \tag{2.5}$$

We assume that the condition (H1) holds and $D \neq 0$. The system (2.4), (2.5) admits $U = 0$ as fixed point, that is, $V(0, \widetilde{\mu}) = 0$. Additionally, the vector field V is reversible, meaning that

$$SV(U, \widetilde{\mu}) = -V(SU, \widetilde{\mu}),$$

where $S = \mathrm{diag}(1, -1, 1, -1)$. In view of these observations, we see that the study of homoclinic solutions of (2.1) via NFT requires first to analyze the linearization of (2.4) at the origin $U = 0$. The characteristic equation is

$$\lambda^4 - B\lambda^2 + A = 0, \tag{2.6}$$

where

$$A = \frac{c_s^2 - c_{\gamma,\delta}^2}{D}, \ B = \frac{(b+d)c_s^2 + (c + a/\varkappa_1)c_{\gamma,\delta}^2}{D}. \tag{2.7}$$

The structure of the spectrum of $L(\widetilde{\mu})$ in (2.4), with D as in (2.5) can be studied following the survey [29]. The distribution of the roots of (2.6) in the (B, A)-plane is given in Fig. 1, which reproduces the bifurcation diagram, along with the location and the type of the four eigenvalues, shown in Figure 1 of [29]. Thus, the behavior of the linear dynamics is determined by the four regions separated by the four bifurcation curves

$$\begin{aligned} \mathbb{C}_0 &= \{(B, A)/A = 0, B > 0\}, \\ \mathbb{C}_1 &= \{(B, A)/A = 0, B < 0\}, \\ \mathbb{C}_2 &= \{(B, A)/A > 0, B = -\sqrt{A}\}, \\ \mathbb{C}_3 &= \{(B, A)/A > 0, B = \sqrt{A}\}. \end{aligned} \tag{2.8}$$

The Center Manifold Theorem and the theory of reversible bifurcations can be applied to study the existence of homoclinic orbits in each bifurcation. The reduced Normal Form systems reveal the existence of homoclinic to zero orbits and homoclinic to periodic orbits. The corresponding solutions are CSW's and GSW's, respectively. In addition, periodic and quasi-periodic orbits are identified, [28].

More specifically, we may adapt the discussion of [29] near the bifurcation curves $\mathbb{C}_0$ to $\mathbb{C}_3$ to the case of (2.4), with D as in (2.5), using (2.3) as bifurcation parameter. Note first that by (2.7), $A = 0$ iff $c_s = c_{\gamma,\delta}$; then $B = S(\gamma, \delta)/(bd - ac/\varkappa_1)$, with $S(\gamma, \delta) := \frac{1+\gamma\delta}{3\delta(\delta+\gamma)}$. Therefore, under the hypothesis (H1), the curve $\mathbb{C}_0$ is characterized by the conditions

$$a, c \leqslant 0, b, d \geqslant 0, bd - \frac{ac}{\varkappa_1} > 0, \ \widetilde{\mu} = 0, \tag{2.9}$$

while the conditions for the curve $\mathbb{C}_1$ are

$$a, c \leqslant 0, b, d \geqslant 0, bd - \frac{ac}{\varkappa_1} < 0. \ \widetilde{\mu} = 0. \tag{2.10}$$

We now study the information furnished by the Normal Form Theory (NFT) close to each curve $\mathbb{C}_j$, $0 \leqslant j \leqslant 3$. In the case of $\mathbb{C}_0$, the linearization matrix $L(0)$ has two simple eigenvalues equal to

$$\pm\sqrt{\frac{S(\gamma, \delta)}{bd - ac/\varkappa_1}}, \tag{2.11}$$

and the zero eigenvalue with geometric multiplicity one and algebraic multiplicity two. As in [28,29], the main role in describing the dynamics close to $\mathbb{C}_0$ by NFT is played by this two-dimensional center manifold. When $\widetilde{\mu}$, A and B are positive, and near $\mathbb{C}_0$ the linear dynamics is given by the spectrum of $L(\widetilde{\mu})$ which consists of four real eigenvalues (region 2 in Fig. 1). In this case, the normal form system has a unique solution, homoclinic to zero at infinity, symmetric and unique up to spatial translations, ([28], Proposition 3.1), that corresponds to a CSW solution of (2.1).

Remark 2.1. If $\widetilde{\mu}$ is negative, by similar arguments to those of [28], NFT establishes the existence of a family of periodic solutions of the reduced system (close to $\mathbb{C}_0$) for each $\widetilde{\mu}$, unique up to spatial translations. For the case at hand, and due to (2.7), if $\widetilde{\mu} < 0$ and $bd - ac/\varkappa_1 > 0$, then $D > 0$. Therefore, $A < 0$ and we fall into region 3 of Fig. 1. Numerical experiments on the generation of approximate periodic traveling wave solutions of (2.1) under these conditions are reported in [2].

In the case of $\mathbb{C}_1$, the spectrum of $L(0)$ consists of zero (with algebraic multiplicity two) and the two simple imaginary eigenvalues given by (2.11) (recall that $bd - ac/\varkappa_1 < 0$). The arguments used in [28], Proposition 3.2, apply here and NFT reduces (2.1), on the center manifold, for $\widetilde{\mu} \neq 0$ small enough, to a normal form system which admits homoclinic solutions to periodic orbits, that is GSW solutions. Information about the structure of the periodic orbits can also be obtained, cf. [30] and references therein.

Remark 2.2. In addition to GSW's, the normal form derived in [28], section 3.2, also reveals the existence of other solutions: periodic, quasi-periodic, and homoclinic to zero solutions (that is, CSW's). This normal form is used in [29] to generalize the result of existence of a homoclinic solution of square hyperbolic secant form (in lowest order of $\widetilde{\mu}$) or a pair of hyperbolic secant solutions close to $\mathbb{C}_1$ and corresponding to region 3 of Fig. 1. As mentioned in [29], persistence of these solutions under small reversible perturbations of the normal form is not expected.

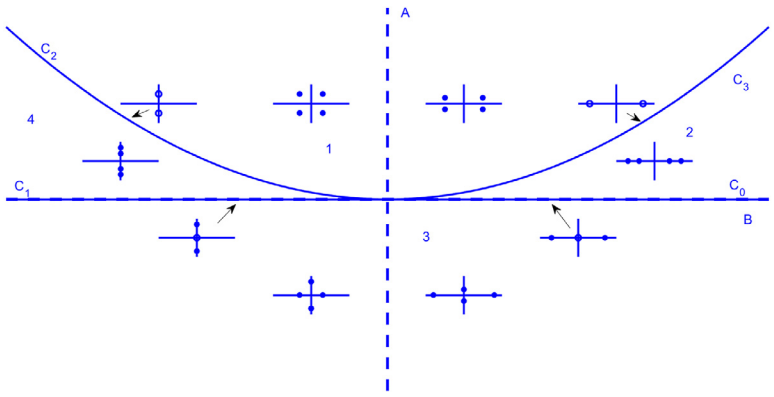

Fig. 1. Linearization at the origin of (2.4) (as in Figure 1 of [29]): Regions 1 to 4 in the (B, A)-plane, delimited by the bifurcation curves $\mathbb{C}_0$ to $\mathbb{C}_3$ given by (2.8), and schematic representation of the position in the complex plane of the roots of (2.6) for each curve and region. (Dot: simple root, larger dot: double root.).

Table 1
Corresponding admissible system in (1.1) and type of solitary waves for small and positive $c_s - c_{\gamma,\delta}$, when $D \neq 0$, according to the Normal Form Theory.

Case	Admissible system	Type of solitary wave
(A1)	$a, c < 0, b = 0, d > 0$	GSW
(A2)	$a, c < 0, b, d > 0, \frac{bd}{\delta+\gamma} - ac < 0$	GSW
(A3)	$a, c < 0, b, d > 0, \frac{bd}{\delta+\gamma} - ac > 0$	CSW
(A4)	$a = 0, c < 0, b, d > 0$	CSW
(A5)	$a < 0, c = 0, b, d > 0$	CSW
(A6)	$a = c = 0, b, d > 0$	CSW

Table 2
Relation between the cases (i)–(vii) of [1], and (A1)–(A6) and $D = 0$ for existence of solitary waves according to the Normal Form Theory.

$(i) \leftrightarrow (A6)$	$\left.\begin{matrix}(iv)\\(vi)\\(vii)\end{matrix}\right\} \leftrightarrow D = 0$
$(ii) \leftrightarrow \begin{cases}(A2)\\(A3)\end{cases}$	
$(iii) \leftrightarrow (A1)$	$(v) \leftrightarrow \begin{cases}(A4)\\(A5)\end{cases}$

The normal form derived in [31] is used in [29] to study the dynamics close to $\mathbb{C}_2$. Its application to our case reveals the existence of homoclinic to zero solutions (CSW's) with nonmonotone decay for $\widetilde{\mu} < 0$ and corresponding to region 1 of Fig. 1 (they have a truncated form like $E_1\,\mathrm{sech}(E_2 x)e^{i\omega\vartheta}$, for constants E_1, E_2 and ω related to the coefficients of the normal form, and $\vartheta \in \mathbb{R}$), and homoclinic solutions to periodic orbits (GSW's) for $\widetilde{\mu} > 0$ corresponding to region 4 of Fig. 1.

Remark 2.3. These CSW's with nonmonotone decay require then speeds c_s smaller than the speed of sound $c_{\gamma,\delta}$ (since $\widetilde{\mu} < 0$) and are different from the CSW's obtained close to $\mathbb{C}_0$, which are strictly positive or negative. The generation and stability of these waves will be examined numerically in Sections 2.2 and 3.3, respectively.

Finally, near $\mathbb{C}_3$, and according to [29], crossing from the region 2 to region 1 in Fig. 1 forms a bifurcation causing the generation of new homoclinic orbits. This bifurcation was analyzed for specific problems, [32–34]. In our case, the numerical computations suggest a similar situation to that described in [32] (see also section 5.1 of [29] and references therein). In particular, CSW's of nonmonotone decay are numerically generated in Section 2.2 (see also [2]).

In summary, NFT establishes the existence of CSW solutions of (2.1) for small and positive $c_s^2 - c_{\gamma,\delta}^2$ when (2.9) holds (close to $\mathbb{C}_0$), and GSW solutions for small $c_s^2 - c_{\gamma,\delta}^2$ under the conditions given in (2.10) and close to $\mathbb{C}_1$. Note that, in the latter case, in view of (1.2), it is not possible to have $a, c < 0, b > 0, d = 0$. Hence, from (2.9) and (2.10), we may distinguish the cases (A1) to (A6) shown in Table 1.

In addition, when $c_s < c_{\gamma,\delta}$, close to $\mathbb{C}_2$, CSW's of nonmonotone decay are shown to exist. They have also been observed numerically close to $\mathbb{C}_3$, cf. Section 2.2. Table 2 shows the relation between the classification (i)–(vii) of parameter cases for the study of well-posedness (cf. the Introduction and [1]) and (A1)–(A6).

For a particular case of $D = 0$ ('classical Boussinesq' $b = 0, d > 0, a = c = 0$) existence and numerical generation of CSW are studied in [35], cf. also [36] for the analogous case of surface waves. In other cases where $D = 0$, numerical evidence of existence of CSW's is presented in [2].

2.1.2. Toland's theory

For larger deviations $c_s - c_{\gamma,\delta}$ or other conditions on the speed c_s, several general theories may be used to analyze the existence of classical solitary waves: Toland's Theory, [18], Concentration–Compactness Theory, [19], and Positive Operator Theory, [20]. In the first case, and in order to apply the results of [18] to study the existence of CSW's, note that system (2.1) may be written in the form

$$S_1\mathbf{v}'' + S_2\mathbf{v} + \nabla g(v_\beta, \zeta) = 0, \tag{2.12}$$

where $\mathbf{v} = (v_\beta, \zeta)^T$ and

$$S_1 = -\begin{pmatrix} \frac{a}{c_s} & b \\ d & \frac{(1-\gamma)c}{c_s} \end{pmatrix}, \quad S_2 = -\begin{pmatrix} \frac{-1}{c_s(\delta+\gamma)} & 1 \\ 1 & -\frac{(1-\gamma)}{c_s} \end{pmatrix}, \tag{2.13}$$

$$g(v_\beta, \zeta) = -\frac{(\delta^2-\gamma)}{c_s(\delta+\gamma)^2}\frac{\zeta v_\beta^2}{2} = -\frac{\varkappa_{\gamma,\delta}}{2c_s}\zeta v_\beta^2,$$

where $\varkappa_{\gamma,\delta}$ is defined in (2.1) and $v_\beta = (1 - \beta\partial_{xx})^{-1}u$. Note that the theory of [18] can be applied here in the symmetric case $b = d$, and may be used to give existence results for classical solitary waves for specific systems in terms of c_s, γ and δ or, alternatively, in terms of $c_s, c_{\gamma,\delta}$, cf. (2.2). We recall the relevant result for existence of solitary waves derived in [18], in the form given in [37].

Theorem 2.1. *Let S_1, S_2 be symmetric, $g \in C^2(\mathbb{R}^2)$ such that $g, \nabla g, \nabla^2 g$ are zero at $(0, 0)$. Let Q and f be given for $\mathbf{u} := (u_1, u_2)^T \in \mathbb{R}^2$ by*

$$Q(\mathbf{u}) = \mathbf{u}^T S_1\mathbf{u}, \; f(\mathbf{u}) = \mathbf{u}^T S_2\mathbf{u} + 2g(\mathbf{u}), \tag{2.14}$$

and assume that:

(I) *$det(S_1) < 0$ and there are two linearly independent vectors $\mathbf{v}_1, \mathbf{v}_2$ such that $Q(\mathbf{v}_1) = Q(\mathbf{v}_2) = 0$.*
(II) *There is a closed plane curve $\mathcal{F}$ with $(0,0) \in \mathcal{F}$ such that*

(i) *$f = 0$ on $\mathcal{F}$ and $\mathcal{F}\backslash\{(0,0)\} \subset \{\mathbf{u} | Q(\mathbf{u}) < 0\}$.*
(ii) *$f(u_1, u_2) > 0$ in the (nonempty) interior of $\mathcal{F}$.*
(iii) *$\mathcal{F}\backslash\{(0,0)\}$ is strictly convex.*
(iv) *$\nabla f(u_1, u_2) = 0$ on $\mathcal{F} \Leftrightarrow (u_1, u_2) = (0,0)$.*

Then there is an orbit $\widetilde{\gamma}$ of (2.12) in the $(v_\beta(0), \zeta)$ plane, which is homoclinic to the origin and

(a) *$(v_\beta(0), \zeta(0)) \in \Gamma$ where Γ is the segment of $\mathcal{F}$ including the origin between P_1, P_2 with P_j satisfying*

$$\langle \nabla f(P_j), \mathbf{v}_j \rangle = 0, \quad j = 1, 2.$$

(b) *v_β, ζ are even functions on $\mathbb{R}$.*
(c) *$(v_\beta(\xi), \zeta(\xi))$ is in the interior of $\mathcal{F}$ for all $\xi \neq 0$.*
(d) *$\widetilde{\gamma}$ is monotone.*

The application of this theory can be made in a similar way to the case of Boussinesq systems for surface waves, [38]. In our context, from (2.12), (2.13) and assuming $a, c \leqslant 0$, $b = d > 0$, we have

$$\begin{aligned} f(v_\beta, \zeta) &= \mathbf{v}^T S_2 \mathbf{v} + 2g(\mathbf{v}) \\ &= \frac{1}{c_s}\left(-\frac{v_\beta^2}{(\delta+\gamma)}\left(1 + \frac{(\delta^2-\gamma)}{(\delta+\gamma)}\zeta\right)\right. \\ &\quad \left. - (1-\gamma)\zeta^2 + 2c_s\zeta v_\beta\right). \end{aligned} \tag{2.15}$$

The quadratic form Q defined in (2.14) is indefinite, and its diagonal form (used to identify two linearly independent directions in which Q vanishes) is of the following types:

(1) If $a < 0$ then

$$Q(U_1, U_2) = -\frac{a}{c_s}U_1^2 + \frac{D}{ac_s}U_2^2,$$

where here $D = b^2c_s^2 - (1-\gamma)ac \geqslant 0$ and

$$U_1 = u_1 + \frac{bc_s}{a}u_2, \quad U_2 = u_2.$$

In this case the two linearly independent directions where $Q = 0$ are given by

$$U_2 = \pm\frac{a}{\sqrt{D}}U_1 \Rightarrow u_2 = \frac{a}{\sqrt{D} - bc_s}u_1, \quad u_2 = -\frac{a}{\sqrt{D} + bc_s}u_1.$$

(2) When $a = 0, c < 0$ then

$$Q(U_1, U_2) = -(1-\gamma)\frac{c}{c_s}U_1^2 + \frac{bc_s}{c(1-\gamma)}U_2^2,$$

with

$$U_1 = u_1 + \frac{bc_s}{c(1-\gamma)}u_2, \quad U_2 = u_2.$$

Now $Q = 0$ when

$$U_2 = \pm\frac{c(1-\gamma)}{c_s\sqrt{b}}U_1 \Rightarrow u_2 = -\frac{c(1-\gamma)}{c_s\sqrt{b}(1+\sqrt{b})}u_1 \quad u_2 = \frac{c(1-\gamma)}{c_s\sqrt{b}(1-\sqrt{b})}u_1.$$

(3) When $a = c = 0$, then $Q(u_1, u_2) = -2bu_1u_2$, and the two independent directions are clearly $u_1 = 0$ and $u_2 = 0$.

As we are investigating existence of classical solitary waves, we will apply Theorem 2.1 for the cases (A3)–(A6) in Table 1. Note that the condition $\det(S_1) < 0$ in (I) of Theorem 2.1 implies that $D > 0$, where D is given by (2.5). By way of illustration, we consider the simplest case (3). The condition $Q < 0$ (see (II)(i) of Theorem 2.1) implies that u_1, u_2 are taken in the first or the third (v_β, ζ) quadrant. The resulting solitary waves are, respectively, of elevation or of depression type, and this is determined by the sign of $\varkappa_{\gamma,\delta}$. Since the linearly independent directions are given in this case by $\mathbf{v}_1 = (1,0)^T$, $\mathbf{v}_2 = (0,1)^T$, the points P_1, P_2 must satisfy

$$f(P_1) = f(P_2) = 0, \quad \frac{\partial f}{\partial u_1}(P_1) = \frac{\partial f}{\partial u_2}(P_2) = 0,$$

which means, following [38],

$$-\varkappa_1 u_1^2 - \varkappa_{\gamma,\delta}u_1^2u_2 - \varkappa_2 u_2^2 + 2c_s u_1 u_2 = 0, \tag{2.16}$$

$$-\varkappa_1 u_1 - \varkappa_{\gamma,\delta}u_1u_2 + c_s u_2 = 0, \tag{2.17}$$

$$-\varkappa_{\gamma,\delta}u_1^2 - 2\varkappa_2 u_2 + 2c_s u_1 = 0, \tag{2.18}$$

where $\varkappa_1 = \frac{1}{\delta+\gamma}$ and $\varkappa_2 = 1-\gamma$. The components of P_1 must satisfy (2.16), (2.17) and those of P_2(2.16), (2.18). Solving (2.16), (2.17) leads to $u_1 = u_2 = 0$ and

$$u_1 = \frac{c_s^2 - c_{\gamma,\delta}^2}{c_s\varkappa_{\gamma,\delta}}, \quad u_2 = \frac{c_s}{\varkappa_2}u_1, \tag{2.19}$$

while solving (2.16), (2.18) yields

$$u_1^\pm = 2\frac{c_s \mp c_{\gamma,\delta}}{\varkappa_{\gamma,\delta}}, \quad u_2^\pm = \pm\sqrt{\frac{\varkappa_1}{\varkappa_2}}u_1^\pm. \tag{2.20}$$

We now consider the components of P_1 and P_2 by using the requirement that they must be in the first or third (v_β, ζ) quadrant. Assume first that $c_s > 0$. Then u_1 and u_2 in (2.19) have always the same sign, while in the case of (2.20) this holds only for u_1^+ and u_2^+. Therefore, P_1 has the components given by (2.19), and from (2.20)$P_2 = (u_1^+, u_2^+)$. It is not hard to check that P_1 and P_2 are in the first (v_β, ζ) quadrant when $(c_s - c_{\gamma,\delta})\varkappa_{\gamma,\delta} > 0$ and in the third quadrant when $(c_s - c_{\gamma,\delta})\varkappa_{\gamma,\delta} < 0$. Then, according to the conclusions of Theorem 2.1, for initial data on $\Gamma = P_1P_2$, the corresponding classical solitary waves are of elevation when $(c_s - c_{\gamma,\delta})\varkappa_{\gamma,\delta} > 0$ and of depression when $(c_s - c_{\gamma,\delta})\varkappa_{\gamma,\delta} < 0$. The orbit $\widetilde{\gamma}$ and the segment Γ for several values of the speed c_s are shown in Figs. 2(a) and (b) respectively.

If we assume that $c_s < 0$, then u_1 and u_2 from (2.19) have always opposite sign. Then necessarily $P_1 = (0,0)$. The same argument as before leads again to obtain $P_2 = (u_1^+, u_2^+)$, with u_1^+, u_2^+ given by (2.20). Furthermore, in this case $c_s - c_{\gamma,\delta}$ is always negative and the condition for P_2 to be in the first or third (v_β, ζ) quadrant depends only on the sign of $\varkappa_{\gamma,\delta}$. For initial data on Γ, the corresponding classical solitary wave is of elevation if $\varkappa_{\gamma,\delta} < 0$ and of depression if $\varkappa_{\gamma,\delta} > 0$.

Remark 2.4. According to the previous arguments based on Toland's theory, the speed c_s must satisfy, in view of the equation $f = 0$, the speed–amplitude relation

$$\begin{aligned} c_s &= \frac{1}{2\mu}\left(\frac{1}{\delta+\gamma}\left(1 + \frac{(\delta^2-\gamma)}{(\delta+\gamma)}\zeta(0)\right) + (1-\gamma)\mu^2\right) \\ &= \frac{1}{2\mu}\left(\varkappa_1 + \varkappa_{\gamma,\delta}\zeta(0) + \varkappa_2\mu^2\right), \end{aligned} \tag{2.21}$$

where $\mu = \zeta(0)/v_\beta(0)$.

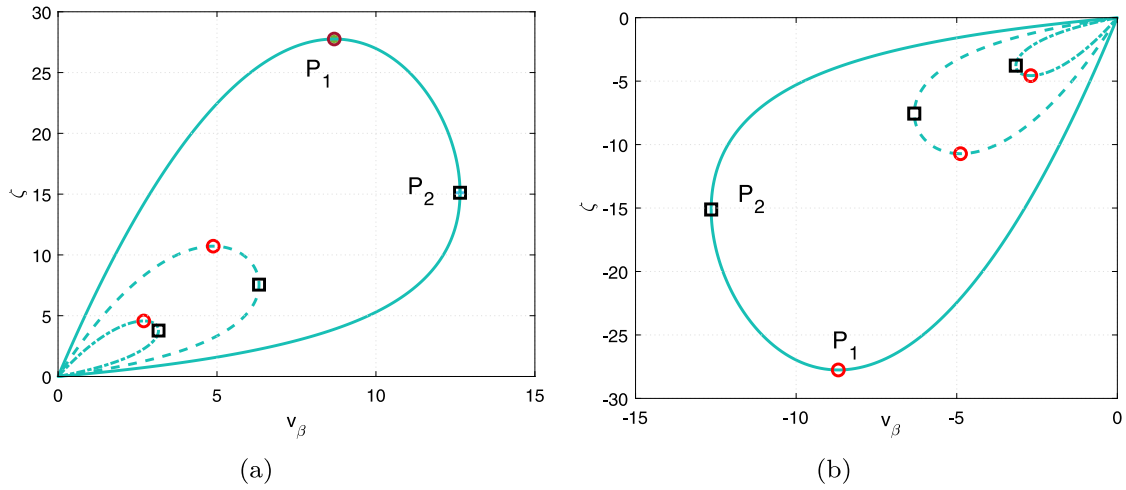

Fig. 2. Generation of CSW's of (a) elevation (case $(c_s - c_{\delta,\gamma})\varkappa_{\gamma,\delta} > 0$) and (b) depression (case $(c_s - c_{\delta,\gamma})\varkappa_{\gamma,\delta} < 0$). Graphs of orbits for several positive values of $c_s - c_{\delta,\gamma}$. Dashed-dotted line: $c_s - c_{\delta,\gamma} = 0.25$; dashed line: $c_s - c_{\delta,\gamma} = 0.5$; solid line: $c_s - c_{\delta,\gamma} = 1$.

2.1.3. Concentration–compactness theory

In the Hamiltonian case ($b = d > 0$) and when $a, c < 0$, another result of existence of CSW's can be obtained from the application of the Concentration–Compactness (C–C) Theory. The method was developed by Lions in [19] and has been used for proving the existence of solitary-wave solutions of a great number of nonlinear dispersive equations. (An exhaustive list of references can be found e. g. in [39]. For the case of Boussinesq systems for surface wave propagation, see [40].) Here, its application is based on identifying solutions of (2.1) with solutions of minimization problems of the form

$$I_r = \inf\{E(\zeta, v) : (\zeta, v) \in H^1 \times H^1 / F(\zeta, v) = r\}, \tag{2.22}$$

for $r > 0$ where, in the case of the B/B systems at hand,

$$E(\zeta, v) = \int_{-\infty}^{\infty} \left(\frac{\varkappa_2}{2} \zeta J_c \zeta + \frac{\varkappa_1}{2} v J_a v - c_s \zeta J_b v \right) dx, \tag{2.23}$$

$$F(\zeta, v) = -\frac{\varkappa_{\gamma,\delta}}{2} \int_{-\infty}^{\infty} \zeta v^2 dx, \tag{2.24}$$

and

$$J_a = 1 + \frac{a}{\varkappa_1}\partial_{xx},\ J_b = 1 - b\partial_{xx},\ J_c = 1 + c\partial_{xx}. \tag{2.25}$$

Existence of CSW's by means of the C–C Theory has been recently proved in [41] for another class of systems modeling internal wave propagation, specifically belonging to the Boussinesq/Full Dispersion (BFD) regime. The proof of [41] can be adapted to the B/B system (2.1) leading to the following result. (The main steps of the proof may be found in [2]).

Theorem 2.2. *Let $\delta > 0, \gamma < 1$ and assume that $a, c < 0, b = d > 0$. If*

$$|c_s| \leqslant M := \min\{\varkappa_2 \frac{|c|}{b}, \frac{|a|}{2b}\}, \tag{2.26}$$

then the system (1.1) admits a classical solitary wave solution $\zeta = \zeta(x - c_s t), v = v(x - c_s t)$ with $(\zeta, v) \in H^\infty \times H^\infty$. Furthermore, ζ and v decay exponentially as $x \to \pm\infty$ with

$$\lim_{x\to\pm\infty} e^{\sigma_a |x|} v(x) = C_1, \tag{2.27}$$

$$\lim_{x\to\pm\infty} e^{\sigma_0 |x|} \zeta(x) = C_2, \tag{2.28}$$

with C_1, C_2 constants, $\sigma_a = \sqrt{\varkappa_1/|a|}$ and $\sigma_0 \in (0, \sigma_a], \sigma_0 < \sqrt{|c|}$.

Remark 2.5. We observe that it is not possible to have $b = d$ in the case (A2) of Table 1. In addition, Theorem 2.2 applies when $|c_s| < c_{\gamma,\delta}$. This should be compared with Toland's theory, cf. Theorem 2.1, for which this condition was not required, cf. [2].

Remark 2.6. In the case of surface waves and Hamiltonian systems there are additional existence and nonexistence results for solitary waves. We first note that similar techniques to the ones we have used here are employed in [40] to prove the existence of solitary waves in the Hamiltonian case $a, c < 0, b = d$ for speeds c_s with $|c_s| < c_0$, where

$$c_0 := \begin{cases} \min\{1, \sqrt{ac}\} & b \neq 0, \\ 1 & b = 0. \end{cases}$$

(In particular, c_s may never reach 1, the speed of sound in this case.) On the other hand, Corollary 1.1 in [11] establishes, in the Hamiltonian case and for some range of values of a, c ('dispersion-like' parameters), among other results, nonexistence of small zero-speed solitary waves, as well as the time interval of existence of small solitary waves with nonzero speed, independently of how small the speed is. These results are revisited in [12], for small $a, c < 0$, Corollary 2.1 asserts the nonexistence of small solitary waves of speed greater than 2 when $a = c$, Theorem 2.2 gives an interval of decay of solutions sharper than that in Corollary 1.1 of [11], precluding the existence of small-speed solitary waves for some range of parameters, and, finally, Corollary 2.2 states that, for any values of $a, c < 0, b$, there are no solitary waves of speed greater than 3.

2.1.4. Positive operator theory

The Positive Operator theory can also be applied as in [42], where some existence results of classical solitary wave solutions of Boussinesq systems for surface waves were derived. In our case, if we take the Fourier transform in (2.1) we obtain

$$\begin{pmatrix} c_s(1 + bk^2) & -\varkappa_1 + ak^2 \\ -\varkappa_2(1 - ck^2) & c_s(1 + dk^2) \end{pmatrix} \begin{pmatrix} \widehat{\zeta}(k) \\ \widehat{v_\beta}(k) \end{pmatrix} = \varkappa_{\gamma,\delta} \begin{pmatrix} \widehat{\zeta v_\beta}(k) \\ \widehat{v_\beta^2/2}(k) \end{pmatrix}. \tag{2.29}$$

System (2.29) is invertible for all $k \in \mathbb{R}$ and for $b, d > 0, a, c \leqslant 0$ if

$$\Delta(k) = \Delta_0 + \Delta_1 k^2 + \Delta_2 k^4 \neq 0, \tag{2.30}$$

where

$$\Delta_0 = c_s^2 - c_{\gamma,\delta}^2, \quad \Delta_1 = c_s^2(b + d) - c_{\gamma,\delta}^2(-c - \frac{a}{\varkappa_1}),$$

$$\Delta_2 = c_s^2 bd - c_{\gamma,\delta}^2 \frac{ac}{\varkappa_1} = c_s^2 bd - (1-\gamma)ac.$$

(Note that Δ_2 is the determinant D given by (2.5).) We assume that $a, c \leqslant 0$, $b, d > 0$, $bd - ac/\varkappa_1 > 0$ (case (A3) of Table 1), and $|c_s| > c_{\gamma,\delta}$. Then $\Delta_j > 0, 0 \leqslant j \leqslant 2$, and we may write (2.29) in the form

$$\widehat{\zeta}(k) = \frac{\varkappa_{\gamma,\delta}}{\Delta(k)}\left(c_s(1+dk^2)\widehat{\zeta v_\beta}(k) + (\varkappa_1 - ak^2)\widehat{v_\beta^2/2}(k)\right)$$
$$\widehat{v_\beta}(k) = \frac{\varkappa_{\gamma,\delta}}{\Delta(k)}\left(c_s(1+bk^2)\widehat{v_\beta^2/2}(k) + \varkappa_2(1-ck^2)\widehat{\zeta v_\beta}(k)\right).$$

As in [42], this leads to an integral form of (2.1)

$$\zeta = k_{12} * (\zeta v_\beta) + \frac{1}{2}k_{22} * (v_\beta^2),$$
$$v_\beta = m_{12} * (\zeta v_\beta) + \frac{1}{2}m_{22} * (v_\beta^2),$$

where the integral kernels are

$$k_{12}(x) = \frac{c_s\varkappa_{\gamma,\delta}}{2\Delta_2}\left(\frac{1-dr_-^2}{r_-(r_+^2-r_-^2)}e^{-r_-|x|} - \frac{1-dr_+^2}{r_+(r_+^2-r_-^2)}e^{-r_+|x|}\right)$$
$$k_{22}(x) = \frac{\varkappa_{\gamma,\delta}}{2\Delta_2}\left(\frac{\varkappa_1+ar_-^2}{r_-(r_+^2-r_-^2)}e^{-r_-|x|} - \frac{\varkappa_1+ar_+^2}{r_+(r_+^2-r_-^2)}e^{-r_+|x|}\right)$$
$$m_{12}(x) = \frac{\varkappa_{\gamma,\delta}}{2\Delta_2}\left(\frac{\varkappa_2(1+cr_-^2)}{r_-(r_+^2-r_-^2)}e^{-r_-|x|} - \frac{\varkappa_2(1+cr_+^2)}{r_+(r_+^2-r_-^2)}e^{-r_+|x|}\right)$$
$$m_{22}(x) = \frac{c_s\varkappa_{\gamma,\delta}}{2\Delta_2}\left(\frac{1-br_-^2}{r_-(r_+^2-r_-^2)}e^{-r_-|x|} - \frac{1-br_+^2}{r_+(r_+^2-r_-^2)}e^{-r_+|x|}\right),$$

with

$$r_\pm^2 = \frac{1}{2\Delta_2}\left(\Delta_1 \pm \sqrt{\Delta_1^2 - 4\Delta_0\Delta_2}\right).$$

When $\varkappa_{\gamma,\delta} > 0$, the Positive Operator theory is applied, as in [42], on the cone of continuous real-valued functions (f, g) on $\mathbb{R}$ which are even, positive and non-increasing on $(0, \infty)$, while if $\varkappa_{\gamma,\delta} < 0$, the cone consists of continuous real-valued functions on $\mathbb{R}$ which are even, negative and non-decreasing on $(0, \infty)$. Then we have

Theorem 2.3. *Assume that $b, d > 0$, $a, c \leqslant 0$, and $bd - ac/\varkappa_1 > 0$. If $|c_s| > c_{\gamma,\delta}$, then the system (2.1) admits classical solitary wave solutions of elevation if $\varkappa_{\gamma,\delta} > 0$ and of depression if $\varkappa_{\gamma,\delta} < 0$.*

Remark 2.7. Note that when $b = d$, Theorem 2.3 reproduces part of the results of Toland's theory in Theorem 2.1.

Remark 2.8. The previous formulas can also be used to estimate the asymptotic decay at infinity of the classical solitary waves. In general, both ζ, v_β should behave as $e^{-r_-|x|}$ as $|x| \to \infty$. In particular, for the cases $b = d > 0$, $a = 0$, $c \leqslant 0$ we may specify r_- in . If $a = 0$, $c < 0$ then

$$\Delta_2 = b^2c_s^2,\ \Delta_1 = 2bc_s^2 + cc_{\gamma,\delta}^2,\ \Delta_0 = c_s^2 - c_{\gamma,\delta}^2,$$

and $\Delta_1^2 - 4\Delta_0\Delta_2 = c^2c_{\gamma,\delta}^4 + 4b(b+c)c_s^2c_{\gamma,\delta}^2 > 0$ (since $b + c = \beta > 0$). Therefore

$$\lim_{x\to\pm\infty} e^{-r_-|x|}v(x) = C,\ r_- = \left(\frac{1}{2\Delta_2}(\Delta_1 - \sqrt{\Delta_1^2 - 4\Delta_0\Delta_2})\right)^{1/2},$$

and C a constant. The argument used in Theorem 2.2 can be applied here as well to obtain (2.28) for some $\sigma_0 \in (0, r_-]$, $\sigma_0 < \sqrt{|c|}$.

On the other hand, if $a = c = 0$, then

$$r_- = \frac{1}{\sqrt{b}}\sqrt{1 - \frac{c_{\gamma,\delta}}{|c_s|}},$$

and in this case

$$\lim_{x\to\pm\infty} e^{-r_-|x|}v(x) = C_1,\ \lim_{x\to\pm\infty} e^{-r_-|x|}\zeta(x) = C_2,$$

for some constants C_1, C_2.

We also note that in [35] existence of even, classical solitary waves of the 'classical Boussinesq' system (case (vii) with $b = 0, d > 0, a = c = 0$, for which $D = 0$) is proved for speeds c_s with $|c_s| > c_{\gamma,\delta}$ and for $\delta^2 - \gamma \neq 0$. The waves are of elevation when $\delta^2 - \gamma > 0$ and of depression otherwise. The result is based on phase plane analysis of the system (2.1), which is conservative in this case; see [43] for the case of surface waves. In addition, for particular values of c_s, some exact formulas for classical solitary wave solutions of (1.1) of sech^2 type may be obtained using similar arguments to those of [37], valid in the case of surface waves. They were derived in [1].

2.2. Numerical generation of solitary waves

In this section some classical and generalized solitary wave profiles will be generated numerically. To this end and following a standard procedure, cf. e. g. [44], the system (2.1) is discretized on a long enough interval $(-l, l)$ and with periodic boundary conditions by the Fourier collocation method based on N collocation points given by $x_j = -l + jh, j = 0, \ldots, N-1$ for an even integer $N \geqslant 1$ and where $h = 2l/N$. If the vectors $\zeta_h = (\zeta_{h,0}, \ldots, \zeta_{h,N-1})^T$ and $v_h = (v_{h,0}, \ldots, v_{h,N-1})^T$ denote, respectively, the approximations to the values of ζ and v_β at the x_j, then the discrete system satisfied by ζ_h and v_h has the form

$$S_N\begin{pmatrix}\zeta_h\\ v_h\end{pmatrix} = \varkappa_{\gamma,\delta}\begin{pmatrix}\zeta_h.v_h\\ (v_h.^2)/2\end{pmatrix}, \tag{2.31}$$

where S_N is the $2N$-by-$2N$ matrix

$$S_N := \begin{pmatrix}c_s(I_N - bD_N^2) & -(\varkappa_1 I_N + aD_N^2)\\ -\varkappa_2(I_N + cD_N^2) & c_s(I_N - dD_N^2)\end{pmatrix}, \tag{2.32}$$

with I_N standing for the N-by-N identity matrix and D_N denoting the N-by-N pseudospectral differentiation matrix (scaled to the interval). The products of the nonlinear terms on the right hand-side of (2.31) are understood in the Hadamard (componentwise) sense. In Section 3, devoted to the computational study of the dynamics of these solitary waves, this method will be used to discretize in space the periodic ivp for (1.1).

The system (2.31), (2.32) is implemented in the Fourier space, that is for the discrete Fourier components of ζ_h and v_h, leading to a 2-by-2 system for each component of fixed-point form

$$S(k)\begin{pmatrix}\widehat{\zeta_h}(k)\\ \widehat{v_h}(k)\end{pmatrix} = \varkappa_{\gamma,\delta}\begin{pmatrix}\widehat{\zeta_h.v_h}(k)\\ \widehat{(v_h.^2)}/2(k)\end{pmatrix}, \tag{2.33}$$

where

$$S(k) = \begin{pmatrix}c_s(1+b\widetilde{k}^2) & -(\varkappa_1 - a\widetilde{k}^2)\\ -\varkappa_2(1-c\widetilde{k}^2) & c_s(1+d\widetilde{k}^2)\end{pmatrix}, \tag{2.34}$$

with $\widetilde{k} = \pi k/l$, $-N/2 \leqslant k \leqslant N/2 - 1$ and $\widehat{\zeta_h}(k)$, $\widehat{v_h}(k)$ denoting, respectively, the kth discrete Fourier component of ζ_h and v_h.

Assuming that $S(k)$ given by (2.34) is nonsingular for all k, $-N/2 \leqslant k \leqslant N/2 - 1$, cf. (2.29), then the system (2.33) is solved iteratively with the Petviashvili scheme, [21,22],

$$S(k)\begin{pmatrix}\widehat{\zeta_h^{[\nu+1]}}(k)\\ \widehat{v_h^{[\nu+1]}}(k)\end{pmatrix} = m_h^2\varkappa_{\gamma,\delta}\begin{pmatrix}\widehat{\zeta_h^{[\nu]}.v_h^{[\nu]}}(k)\\ \widehat{((v_h^{[\nu]}).^2)}/2(k)\end{pmatrix},$$
$$\nu = 0, 1, \ldots,\ -N/2 \leqslant k \leqslant N/2 - 1, \tag{2.35}$$

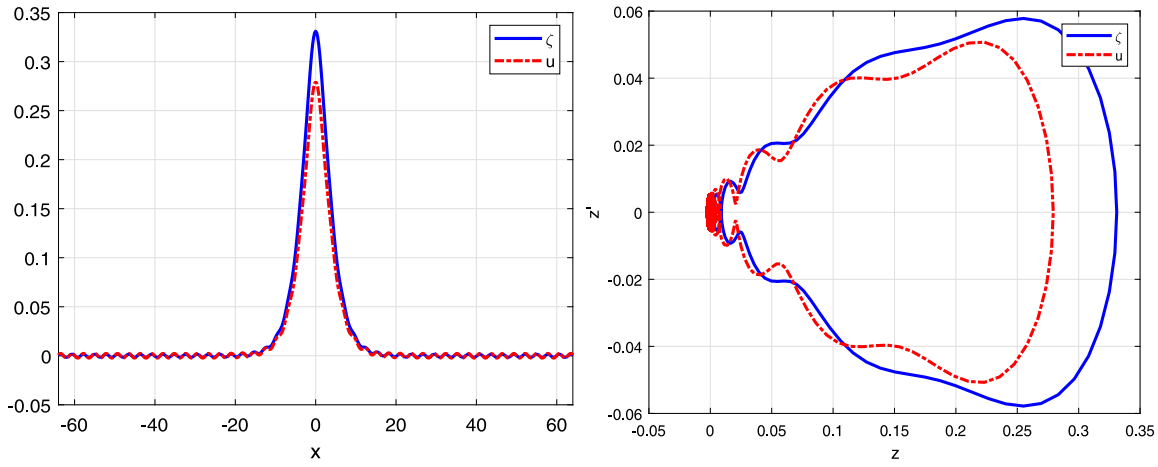

Fig. 3. GSW generation. Case (A1) with $\delta = 0.9, \gamma = 0.5, c = -1/3, b = 0, d = 1, a = \varkappa_1(S(\gamma,\delta) - b - c - d) \approx -0.2022$; $c_s = c_{\gamma,\delta} + 0.02 \approx 0.6176$. (a) ζ and u profiles; (b) ζ and u phase portraits.

where m_h is the corresponding stabilizing factor

$$m_h = \left(S_N \begin{pmatrix} \zeta_h^{[\nu]} \\ v_h^{[\nu]} \end{pmatrix}, \begin{pmatrix} \zeta_h^{[\nu]} \\ v_h^{[\nu]} \end{pmatrix}\right)_N \Big/ \left(\begin{pmatrix} \zeta_h^{[\nu]}.v_h^{[\nu]} \\ ((v_h^{[\nu]}).^2/2)(k) \end{pmatrix}, \begin{pmatrix} \zeta_h^{[\nu]} \\ v_h^{[\nu]} \end{pmatrix}\right)_N,$$

with $(\cdot,\cdot)_N$ denoting the Euclidean inner product in $\mathbb{C}^{2N}$. The iterative procedure (2.35) is in some cases accelerated by using vector extrapolation methods, [23]. For the application of these techniques to the Petviashvili method for traveling wave computations see [45]. The benefits of their use include a reduction in the number of iterations when Petviashvili's method is convergent, and the transformation of divergent cases into convergent. Once the iteration is completed and approximations ζ_h and v_h have been computed, an approximation of $u = (1 - \beta\partial_{xx})v_\beta$ can be obtained as $u_h = (I_N - \beta D_N^2)v_h$.

Some details on the implementation are now given. For the experiments below h varies in a range between 6.25×10^{-2} and 2.5×10^{-1}. In all the computations the approximate profiles for ζ and u and corresponding phase portraits are displayed. The accuracy of the profiles is monitored in two ways. First, the behavior of the residual error at each iteration

$$RES(\nu) = \left\| S_N \begin{pmatrix} \zeta_h^{[\nu]} \\ v_h^{[\nu]} \end{pmatrix} - \begin{pmatrix} \zeta_h^{[\nu]}.v_h^{[\nu]} \\ ((v_h^{[\nu]}).^2)/2 \end{pmatrix} \right\|, \tag{2.36}$$

where $\|\cdot\|$ denotes the Euclidean norm, is checked. The residual error also controls the iteration, which is run while *RES* is above a prefixed tolerance (or, by defect, a maximum number of iterations is not attained). A second test of accuracy consists of integrating numerically the periodic ivp of (1.1) by some fully discrete scheme, with the computed profiles as initial condition, and monitoring several error indicators during the evolution of the corresponding numerical solution. This was performed in the first part of the study, [1] (see also [2]), using a fully discrete scheme based on a Fourier pseudospectral discretization in space and, as time integrator, a fourth-order Runge–Kutta (RK)-composition method based on the implicit midpoint rule. The fully discrete method and the evolution experiments will be used in Section 3 in the sequel for the computational study of the solitary wave dynamics.

In the rest of the present section we illustrate several cases of numerically generated solitary waves. In each one of the figures we present the profiles of the ζ- and u-solitary waves, and their phase space diagrams. We refer to the extended version of the paper, [2], for more experiments and more details on the tests for accuracy monitoring (2.36) and on the fully discrete scheme.

We start with an illustration of GSW's, predicted by NFT. Fig. 3 corresponds to the case (A1) with

$$\delta = \gamma = 0.5, c = -1/3, b = 0, d = 1,$$
$$a = \varkappa_1(S(\gamma,\delta) - b - c - d) \approx -0.2022.$$

The speed is $c_s = c_{\gamma,\delta} + 0.02 \approx 0.6176$. A wave of elevation results and the corresponding phase portrait shows how the profile is homoclinic to a periodic orbit at infinity. We checked that this homoclinic orbit corresponds to region 3 of Fig. 1. (In the phase portrait part of this and subsequent similar figures, the horizontal axis z depicts the solitary-wave profiles ζ, resp. u, and the vertical axis $z' = z_x$ depicts ζ_x, resp. u_x.)

We turn now to the numerical generation of CSW's. First we illustrate the cases (A3)–(A6) of Table 1 with examples that are covered by the other three theories considered in Section 2.1, namely Toland's Theory, Concentration–Compactness Theory and Positive Operator Theory. The associated homoclinic orbits correspond to region 2 of the (B, A)-plane in Fig. 1.

The case (A3) is exemplified in Figs. 4 and 5. In Fig. 4, we took $\delta = 0.9, \gamma = 0.5, a = -1/3, c = -2/3, b = 1/3, d = -(\delta+\gamma)a - b - c + \frac{1+\gamma\delta}{3\delta(\gamma+\delta)} \approx 1.1836$, and $c_s = c_{\gamma,\delta} + 0.5 \approx 1.0976$. The resulting classical solitary wave is of elevation type. It was also checked that $\Delta_j > 0, 0 \leqslant j \leqslant 3$, where Δ_j are given by (2.30). Hence this example illustrates Theorem 2.3, i. e. is an application of Positive Operator Theory to (2.1). On the other hand, an application of Theorem 2.2, deduced from the Concentration–Compactness Theory, is shown in Fig. 5. In this case, with the same values of δ and γ, a, and c, but different b and d, the computed CSW is of depression type and has speed $c_s = c_{\gamma,\delta} - 0.25 \approx 0.3476$.

Toland's theory may justify the example of Fig. 6, corresponding to a Hamiltonian case of (A6). The numerical experiment is performed using a variant of the Petviashvili method (2.35) as follows. For a fixed speed c_s, each iterate $(v_h^{[\nu]}, \zeta_h^{[\nu]})$ of the method is forced to be in the manifold $\{f = 0\}$, where f is given by (2.15). This is accomplished by complementing the Petviashvili iteration with a projection method, implemented in the standard way, [46]. For the particular example of Fig. 6, with speed $c_s = c_{\gamma,\delta} + 0.5$, the points P_1 and P_2 of the segment Γ, cf. Theorem 2.1, have the components (approximately)

$$P_1 = (4.8825, 10.7182), \ P_2 = (6.3226, 7.5569),$$

and the computed solitary wave profile has amplitude $\zeta_{max} \approx 9.7566$ with $v_{max} \approx 5.9357$ and $u_{max} \approx 6.7788$.

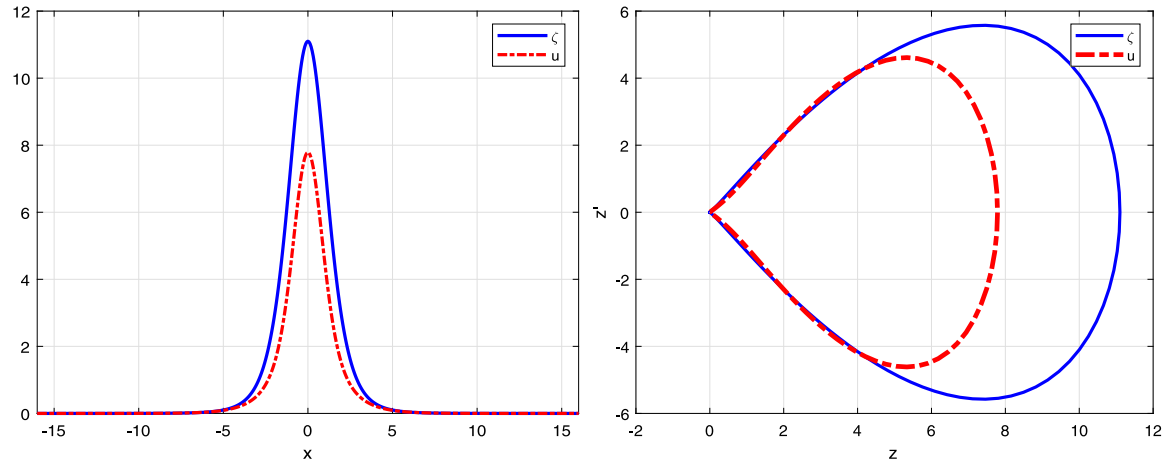

Fig. 4. CSW generation. Case (A3) with $\delta = 0.9$, $\gamma = 0.5$, $a = -1/3$, $c = -2/3$, $b = 1/3$, $d = -(\delta+\gamma)a - b - c + \frac{1+\gamma\delta}{3\delta(\gamma+\delta)} \approx 1.1836$; $c_s = c_{\gamma,\delta} + 0.5 \approx 1.0976$. (a) ζ and u profiles; (c) ζ and u phase portraits.

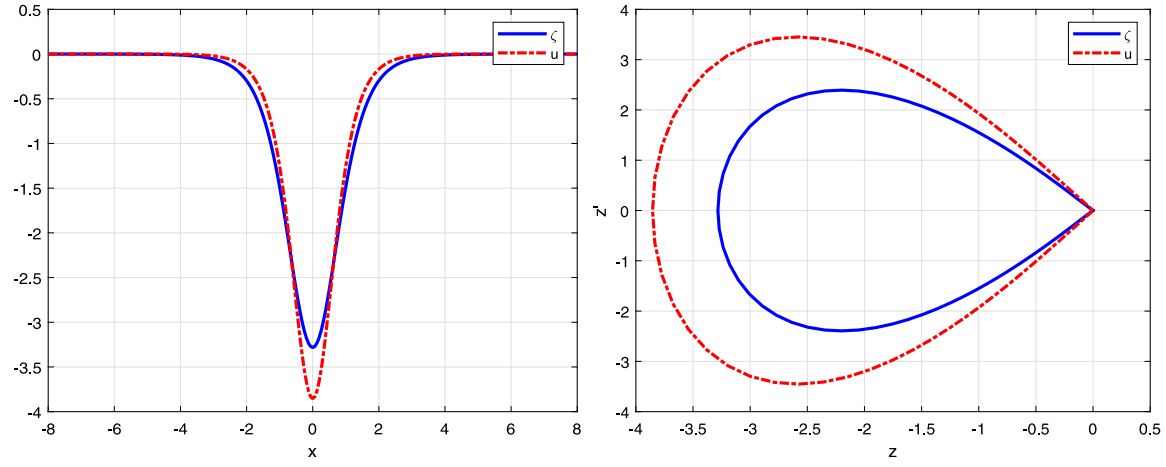

Fig. 5. CSW generation. Case (A3) with $\delta = 0.9$, $\gamma = 0.5$, $a = -1/3$, $c = -2/3$, $b = d = \frac{1}{2}(-(\delta+\gamma)a - c + \frac{1+\gamma\delta}{3\delta(\gamma+\delta)}) \approx 0.7585$; $c_s = c_{\gamma,\delta} - 0.25 \approx 0.3476$. (a) ζ and u profiles; (c) ζ and u phase portraits.

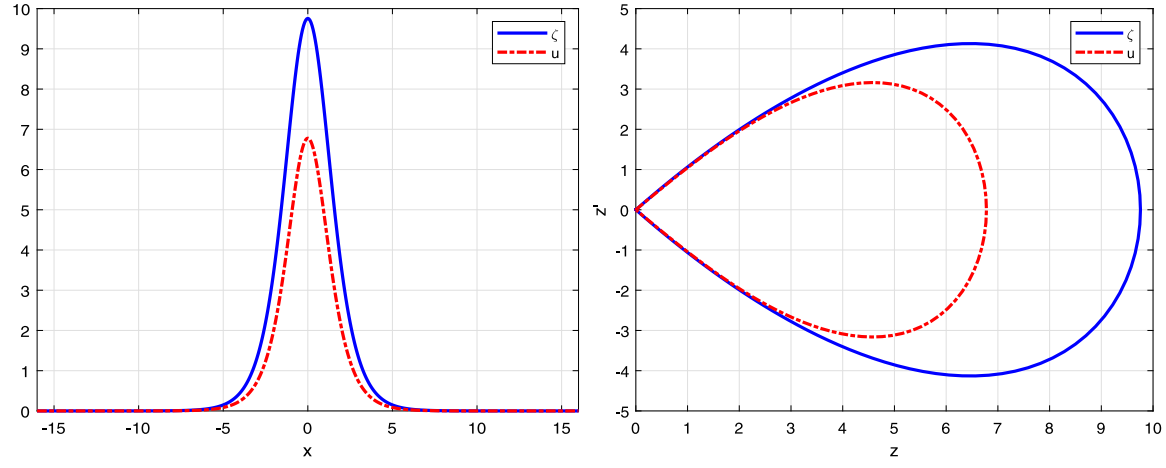

Fig. 6. CSW generation. Case (A6) with $\delta = 0.9$, $\gamma = 0.5$, $a = 0$, $c = 0$, $b = d = \frac{1}{2}\frac{1+\gamma\delta}{3\delta(\gamma+\delta)} \approx 0.1918$; $c_s = c_{\gamma,\delta} + 0.5 \approx 1.0976$. (a) ζ and u profiles; (c) ζ and u phase portraits.

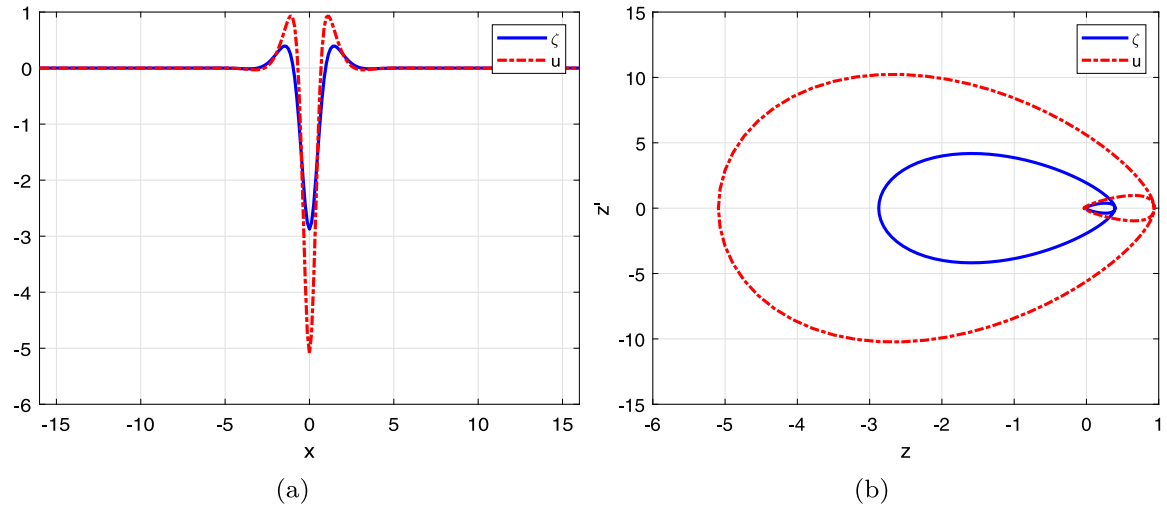

Fig. 7. CSW generation with $a = -1/9, c = -1/6, b = 0, d = -a/\varkappa_1 - c - b + S(\gamma, \delta) \approx 0.7058, \delta = 0.9, \gamma = 0.5$, and speed $c_s = c_{\gamma,\delta} - 0.2 \approx 3.9761 \times 10^{-1}$ (a) ζ and u profiles; (c) ζ and u phase portraits.

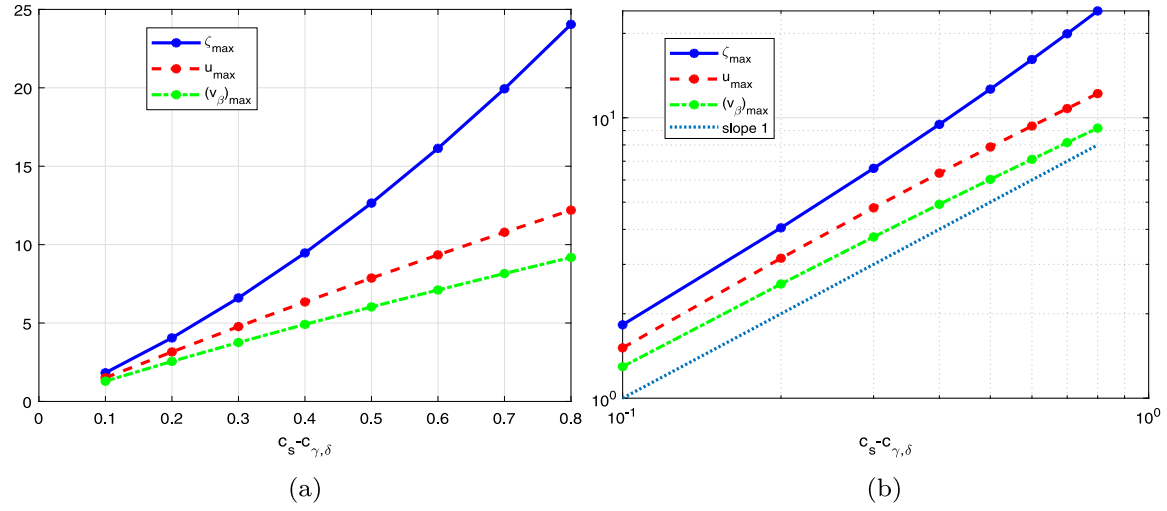

Fig. 8. Speed–amplitude relation in (a) linear scale and (b) log–log scale. Case (A6) with $\delta = 0.9, \gamma = 0.5, a = 0, c = 0, b = d = \frac{1}{2}\frac{1+\gamma\delta}{3\delta(\gamma+\delta)}$.

Recall that the theories examined in this paper exclude the case $D = 0$, where D is given by (2.5). However, some numerical experiments in that case suggest existence of classical solitary waves. These may be seen in [2]. (Existence of CSW's for the particular case of the 'classical Boussinesq' system, with $b = 0, d > 0, a = c = 0$, is a special case and is proved e. g. in [35].)

We complete this numerical study by illustrating the generation of CSW's with non-monotonic decay predicted by NFT. An example appears in Fig. 7, which corresponds to a homoclinic orbit belonging to the first-quadrant part of region 1 in Fig. 1 and to the values

$$a = -1/9, c = -1/6, b = 0,$$
$$d = -a/\varkappa_1 - c - b + S(\gamma, \delta) \approx 0.7058, \delta = 0.9, \gamma = 0.5,$$

and speed $c_s = c_{\gamma,\delta} - 0.2 \approx 3.9761 \times 10^{-1}$. (A nonmonotone CSW corresponding to the second quadrant of region 1 was also generated, cf. [2].)

The last experiment in this section concerns the speed–amplitude relation. Fig. 8 displays, in linear and log–log scales and for fixed γ, δ, the amplitude of the computed profiles for ζ, u and v_β as functions of the difference $c_s - c_{\gamma,\delta}$. The results correspond to an experiment with $\delta = 0.9, \gamma = 0.5$ and parameters $a = c = 0, b = d = \frac{1}{2}\frac{1+\gamma\delta}{3\delta(\gamma+\delta)}$ (case (A6) of Table 1 with Hamiltonian structure). Similar experiments were made for different parameters leading to other CSW's (including those of nonmonotone decay) as well as GSW's, and the results resemble qualitatively those of this figure. The three maximum values (for ζ, u and v_β) are increasing functions of $c_s - c_{\gamma,\delta}$, with the amplitude of ζ increasing faster. Fig. 8(b), in log–log scale, includes a dotted line of slope 1 for comparison purposes. The representation of the amplitudes as affine functions for small $c_s - c_{\gamma,\delta}$ seems to fit the results (as expected). For larger values of $c_s - c_{\gamma,\delta}$, the slope of the line for the ζ-amplitude is increasing faster while the approximate linear fitting persists longer for the velocity variables.

3. Computational study of solitary wave dynamics

In this section we present a computational study of the dynamics of some aspects of solitary waves, both classical and generalized. To this end, and as mentioned in the introduction, the periodic ivp for (1.1) on a long enough interval was discretized in space by a Fourier spectral method and in time by a fourth-order RK-composition method, cf. [1], where the resulting fully discrete scheme was introduced and its accuracy was checked with several numerical examples.

In the present case the procedure, described in Section 2.2, for the numerical generation of solitary waves suggests implementing the spatial discretization in collocation form. Thus, for $T > 0$ and using the notation of Section 2.2, the semidiscrete solution (ζ_N, v_N) satisfying (1.1) at the collocation points x_j is represented by the vectors of nodal values

$$Z_N(t) = (\zeta_N(x_j,t))_{j=0}^{N-1},\ V_N(t) = (v_N(x_j,t))_{j=0}^{N-1},\ 0 \leqslant t \leqslant T,$$

that are solutions of the semidiscrete system

$$\begin{aligned}(I_N - bD_N^2)\frac{d}{dt}Z_N + \varkappa_1(I_N + \frac{a}{\varkappa_1}D_N^2)D_N V_N \\ + \varkappa_{\gamma,\delta} D_N(Z_N.V_N) = 0,\\ (I_N - dD_N^2)\frac{d}{dt}V_N + (1-\gamma)(I_N + cD_N^2)\\ \times D_N Z_N + \varkappa_{\gamma,\delta} D_N(\frac{V_N.^2}{2}) = 0,\end{aligned} \tag{3.1}$$

for $0 \leqslant t \leqslant T$ and where I_N and D_N are defined in (2.32). The ode system (3.1) is integrated numerically in time with the 4*th*-order, 3-stage Runge–Kutta-composition method based on the implicit midpoint rule, cf. [13,46].

The *generic case* $(a, c < 0, b, d > 0)$ is considered for the experiments. In this case we have existence of classical solitary waves when $\varkappa_1 bd - ac > 0$ (case (A3) of Table 1) and of generalized solitary waves when $\varkappa_1 bd - ac < 0$ (case (A2) of Table 1). For the computations in this section, we use the same values of the stepsizes, mainly $h = 1.25 \times 10^{-1}$, $\Delta t = 6.25 \times 10^{-3}$, changing the interval parameter L and the number N of collocation points in order to maintain the same h up to the final time of integration.

3.1. CSW dynamics. Numerical experiments

The experiments in this section concern the evolution of solutions emanating from small and larger perturbations of CSW's, as well as head-on and overtaking collisions of CSW's. For simplicity, only the results for the numerical ζ-component ζ_N will be shown.

3.1.1. Small perturbations of a CSW

In order to illustrate the evolution of a perturbed CSW in the generic case, we take the specific values

$$\begin{aligned}&\gamma = 0.5, \delta = 0.9, a = -1/3, c = -2/3, b = 1/3,\\ &d = -\frac{a}{\varkappa_1} - b - c + \frac{1+\gamma\delta}{3\delta(\gamma+\delta)} \approx 1.1836.\end{aligned} \tag{3.2}$$

A typical experiment consists of generating a corresponding approximate CSW profile (ζ_h, u_h) for these values (here with specific data $l = 256$, $N = 4096$, $c_s = c_{\gamma,\delta} + 0.1 \approx 0.6976$, starting from a sech^2-initial profile), taking a perturbation

$$\zeta_N(0) = A\zeta_h,\ u_N(0) = Au_h, \tag{3.3}$$

with A constant as initial condition and monitoring the resulting numerical solution up to some final time T, which was taken in the experiments to be up to $T = 800$. The time step was $\Delta t = 6.25 \times 10^{-3}$.

For $A = 1.1$ the results are given in Figs. 9 and 10. Fig. 9 shows the evolution of the numerical approximation at several time instances. In this small perturbation case, a new CSW emerges, with a small-amplitude tail of dispersive nature following the main wave and shown in detail in Fig. 9(d).

The structure of such dispersive tails can be analyzed from the behavior of small-amplitude solutions of the linearized system associated to (1.1) in a frame $y = x - c_s t$ moving with the speed c_s of the CSW, given by

$$(1 - b\partial_{yy})(\partial_t - c_s\partial_y)\zeta + \varkappa_1\partial_y J_a v_\beta = 0, \tag{3.4}$$

$$(1 - d\partial_{yy})(\partial_t - c_s\partial_y)v_\beta + \varkappa_2\partial_y J_c\zeta = 0, \tag{3.5}$$

where J_a, J_c are given by (2.25). Applying the operator $(1 - d\partial_{yy})(\partial_t - c_s\partial_y)$ to (3.4) and using (3.5) we obtain the high-order wave equation

$$(1 - d\partial_{yy})(1 - b\partial_{yy})(\partial_t - c_s\partial_y)^2\zeta - \varkappa_1\varkappa_2\partial_y^2 J_a J_c\zeta = 0. \tag{3.6}$$

Plane wave solutions $\zeta(y,t) = e^{i(ky-\omega(k)t)}$ of (3.6) satisfy the linear dispersion relation

$$\omega(k) = \omega_\pm(k) = -kc_s \pm c_{\gamma,\delta}k\phi(k^2),$$

where $\phi : [0,\infty) \to \mathbb{R}$ is the function

$$\phi(x) = \sqrt{\frac{(1-\widetilde{a}x)(1-cx)}{(1+bx)(1+dx)}},\ \widetilde{a} = \frac{a}{\varkappa_1}.$$

This leads to a local phase speed (relative to the speed of the CSW)

$$v_\pm(k) = -c_s \pm c_{\gamma,\delta}\phi(k^2). \tag{3.7}$$

Some properties of the function ϕ can explain the behavior of (3.7). These are:

(1) $\phi(x) \geqslant 0, x \geqslant 0,\ \phi(0) = 1.$
(2) From the condition $\varkappa_1 bd - ac > 0$, characterizing (A3), we have
$$\lim_{x\to\infty}\phi(x) = \phi_* := \sqrt{\frac{ac}{\varkappa_1 bd}} < 1.$$
(3) Let
$$\begin{aligned}p_1 &= \widetilde{a}c(b+d) + bd(\widetilde{a}+c),\\ p_2 &= 2(\widetilde{a}c - bd) < 0 \text{ (cf. (A3))},\\ p_3 &= \frac{1+\gamma\delta}{3\delta(\gamma+\delta)} > 0.\end{aligned} \tag{3.8}$$
Then
$$\phi'(x) = \frac{P(x)}{2\phi(x)(1+bx)^2(1+dx)^2},\ P(x) = p_1x^2 + p_2x - p_3. \tag{3.9}$$
Therefore, the monotonicity of ϕ depends on the polynomial $P(x)$, in particular on the sign of p_1. Let $\Delta = p_2^2 + 4p_1p_3$ be the discriminant of the equation $P(x) = 0$. Then we have the cases:

(i) $p_1 < 0$. In this case $\Delta \leqslant 0$. Then $P(x)$ has the same sign for all $x \geqslant 0$. Since $P(0) = -p_3 < 0$, then $P(x) < 0, x \geqslant 0$. Therefore, $\phi(x)$ is decreasing for $x \geqslant 0$. On the other hand, when $\Delta = 0$ then $P(x)$ has a double root at $x = x_* = -p_2/2 > 0$, where $P(x)$ attains a minimum. Thus:
  (1) If $0 \leqslant x \leqslant x_*$, then $\phi(x)$ is decreasing with $1 > \phi(x) \geqslant \phi(x_*)$.
  (2) If $x_* \leqslant x$, then $\phi(x)$ is increasing with $\phi(x_*) \leqslant \phi(x) \leqslant \phi_* < 1$.

(ii) $p_1 = 0$. In this case $P(x) = p_2x - p_3$ has only the root $x = p_3/p_2 < 0$ and therefore $\phi(x)$ is decreasing for $x > 0$ with $0 \leqslant \phi(x) \leqslant \phi(0) = 1$.

(iii) $p_1 > 0$. This implies $\Delta > 0$ and the existence of two simple roots of $P(x)$, one positive $x_* = \frac{1}{2}(-p_2 + \sqrt{\Delta})$ and one negative. The behavior is then similar to the case $\Delta = 0$ in (i), that is
  (1) If $0 \leqslant x \leqslant x_*$, then $\phi(x)$ is decreasing with $1 > \phi(x) \geqslant \phi(x_*)$.

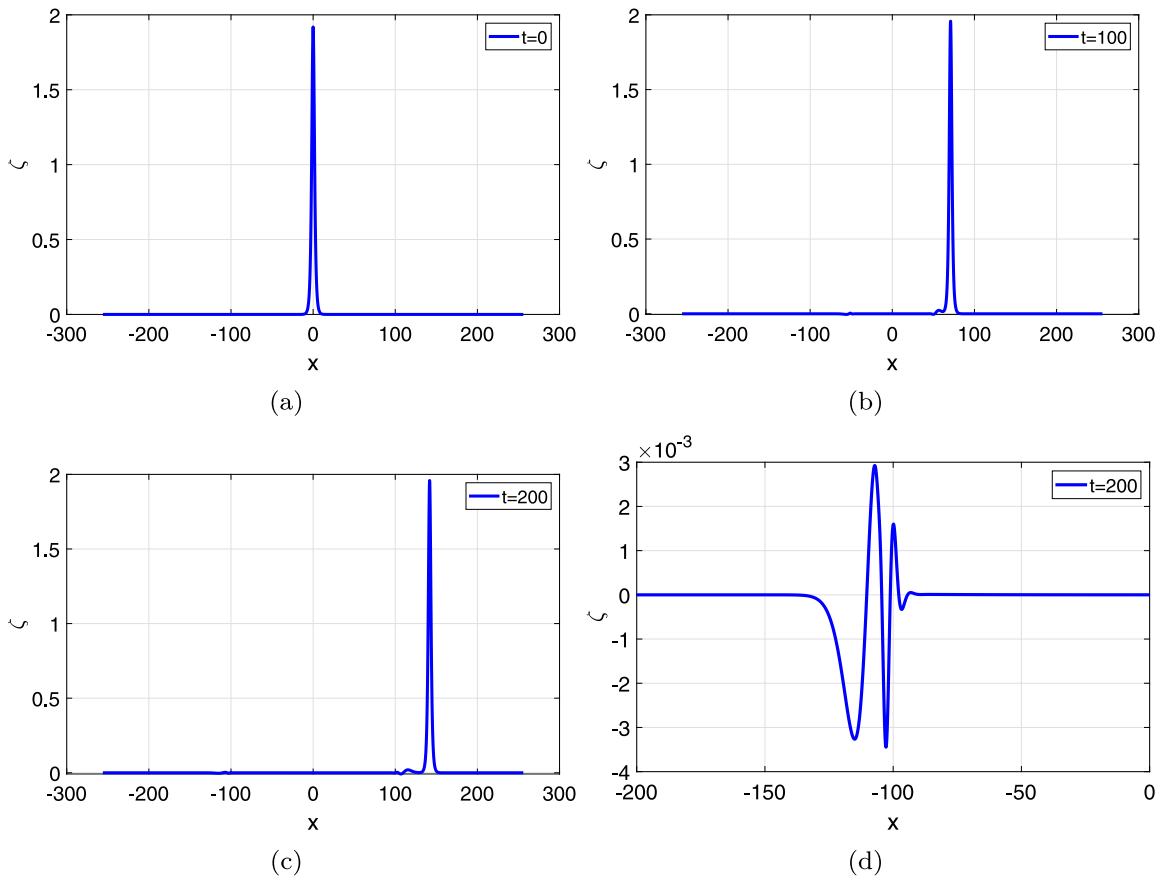

Fig. 9. Evolution of a CSW perturbed slightly. Case (A3) with (3.2), (3.3) $A = 1.1, c_s = c_{\gamma,\delta} + 0.1$. (a)–(c) ζ component of the numerical solution; (d) Magnification of (c) between $x = -200$ and $x = 0$.

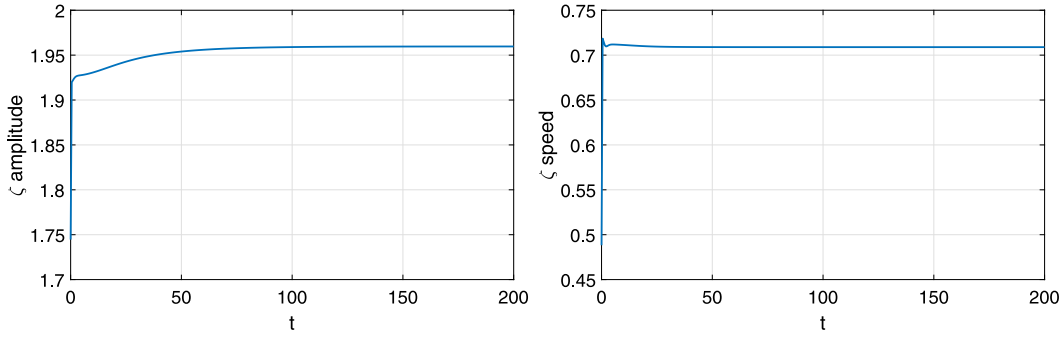

Fig. 10. Evolution of a CSW perturbed by a small amount. Case (A3) with (3.2), (3.3) $A = 1.1, c_s = c_{\gamma,\delta} + 0.1$. Evolution of amplitude and speed of the ζ component of the main pulse.

(2) If $x_* \leqslant x$, then $\phi(x)$ is increasing with $\phi(x_*) \leqslant \phi(x) \leqslant \phi_* < 1$.

With all these properties we have

$$-c_s - c_{\gamma,\delta} < v_-(k) < -c_s < v_+(k) < -c_s + c_{\gamma,\delta}.$$

If we assume $c_s > c_{\gamma,\delta}$, then we conclude that plane wave components of the dispersive tail, traveling to the right or to the left, trail the solitary wave with an absolute phase speed satisfying $v_+(k) + c_s < c_{\gamma,\delta}$ and $|v_-(k) + c_s| < c_{\gamma,\delta}$. Furthermore, components with smaller k (long wavelength) are faster than those with larger k (short wavelength).

For the group velocities we have

$$\omega'_\pm(k) = -c_s \pm c_{\gamma,\delta}\psi(k^2),$$

where $\psi : [0, \infty) \to \mathbb{R}$ is the function

$$\psi(x) = 2x\phi'(x) + \phi(x), \tag{3.10}$$

The behavior in this case seems to be similar to that of ϕ, cf. [2]. Different values of the parameters (always in the generic case and with the condition $\varkappa_1 bd - ac > 0$) seem to suggest the existence of a minimum, to the left of which $0 \leqslant \psi(x) \leqslant 1$ and after which ψ grows up to

$$\lim_{x\to\infty} \psi(x) = \phi_* := \sqrt{\frac{ac}{\varkappa_1 bd}} < 1.$$

Under these conditions, we would have

$$-c_s - c_{\gamma,\delta} < \omega'_-(k) < -c_s < \omega'_+(k) < -c_s + c_{\gamma,\delta}.$$

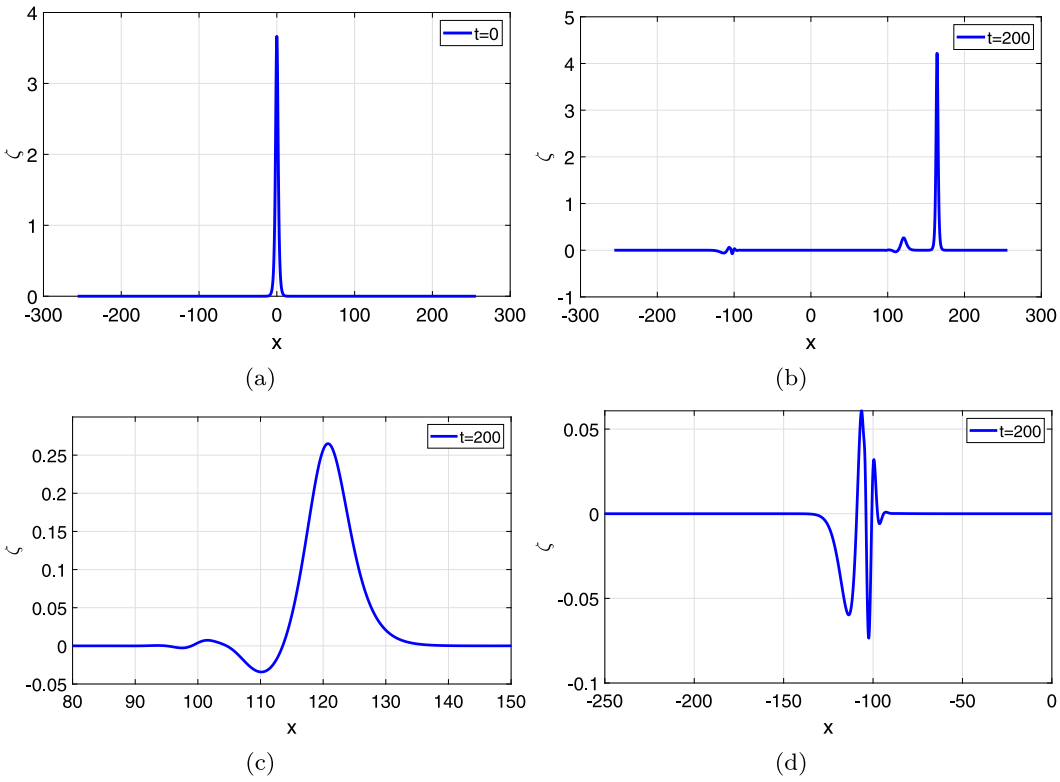

Fig. 11. Evolution of a perturbed CSW. Case (A3) with (3.2), (3.3) $A = 2.1$, $c_s = c_{\gamma,\delta} + 0.1$. (a), (b) ζ component of the numerical solution; (c) First structure of the ζ component of the numerical solution; (d) Second structure.

If we assume $c_s > c_{\gamma,\delta}$ again, this would imply the existence of two dispersive groups, one traveling to the left and one to the right following the solitary wave, with group velocity smaller than c_s with $|\omega'_{\pm}(k) + c_s| < c_{\gamma,\delta}$. In Fig. 9(c) a first tail, close to the main wave and traveling to the right is observed, while a second wave packet of smaller amplitude appears in the magnified Fig. 9(d). At $t = 200$, this wavelet is traveling to the left with effective support in $[-130, -90]$ (cf. [47] for a similar wavelet in some cases of surface waves).

Finally, Fig. 10 shows the evolution of the amplitude and speed of the ζ component of the numerical approximation of the main pulse for the system with parameters given by (3.2). In this example, the emerging solitary wave is faster and larger than the perturbed initial profile.

Remark 3.1. A similar study can also be applied to the rest of the cases (A4)–(A6) of Table 1. Thus, in the cases (A4) and (A5), we have $p_1 < 0$, while in the case (A6), $p_1 = 0$. Then, analogous results to those of the generic case (A3) of CSW's hold.

3.1.2. Larger perturbation of a CSW

Increasing the value of the perturbation parameter A leads, in our example, to the generation of another solitary wave; no instability was observed. Fig. 11 illustrates the experiment with $A = 2.1$ (the spatial and temporal step sizes are the same as those of the previous experiments). The evolution of the numerical approximation (see Fig. 11(a), (b)) shows, in addition to the generation of a dominant, emerging solitary wave, (a bit taller than that of the perturbed initial data for the example at hand, cf. [2]), the formation of two other structures. Immediately behind the main wave, a nonlinear wave of solitary-wave type seems to be forming, along with a dispersive tail trailing it and traveling to the right, as Fig. 11(c) reveals. The nature of the second structure on the left of the main wave (see the magnification in Fig. 11(d)) is not so clear. Apparently, the wave contains some dispersive component (as in the experiment with small perturbations in the previous section) but its persistence during the evolution may suggest the existence of something that does not disperse strongly. Similar conclusions hold from the experiments (not shown here) with $A = 3.1$. This behavior also suggests, as the structure seems to be moving to the left, the formation of a wavelet, or a superposition of them, such as observed in Boussinesq systems for surfaces waves, see e. g. [48]. Nevertheless, the possibility of the formation of a CSW with nonmonotone decay is not to be discarded.

These observations persist when the value of A is taken to be larger. In order to illustrate this, we show the analogous experiment corresponding to $A = 6.1$, in Fig. 12. For this larger perturbation, the initial perturbed wave gives rise to a main solitary-wave pulse and seems to exhibit a sort of stronger resolution property, with a solitary wave of elevation forming behind and following the main wave, see Fig. 12(c). As for the second structure, the possible formation of a CSW of depression with nonmonotone decay is more clearly observed (Fig. 12(d)) than in the previous experiment.

3.1.3. Overtaking collisions

Overtaking collisions are illustrated in the following experiment. With the same values of the parameters given by (3.2), we generate two approximate CSW profiles with speed $c_s^{(1)} = c_{\gamma,\delta} + 0.5 \approx 1.0976$ centered at $x_0^{(1)} = 0$, and speed $c_s^{(2)} = c_{\gamma,\delta} + 0.2 \approx 0.7976$ centered at $x_0^{(2)} = 20$, respectively. The superposition of these profiles is taken as initial condition for the numerical method. The ensuing evolution is shown in Fig. 13(a) and (b), while Fig. 13(c) and (d) are magnifications of 13(b).

The experiment shows that after the one-way collision, two solitary waves emerge. The amplitude of the larger one, compared to that of the corresponding wave before the collision, has

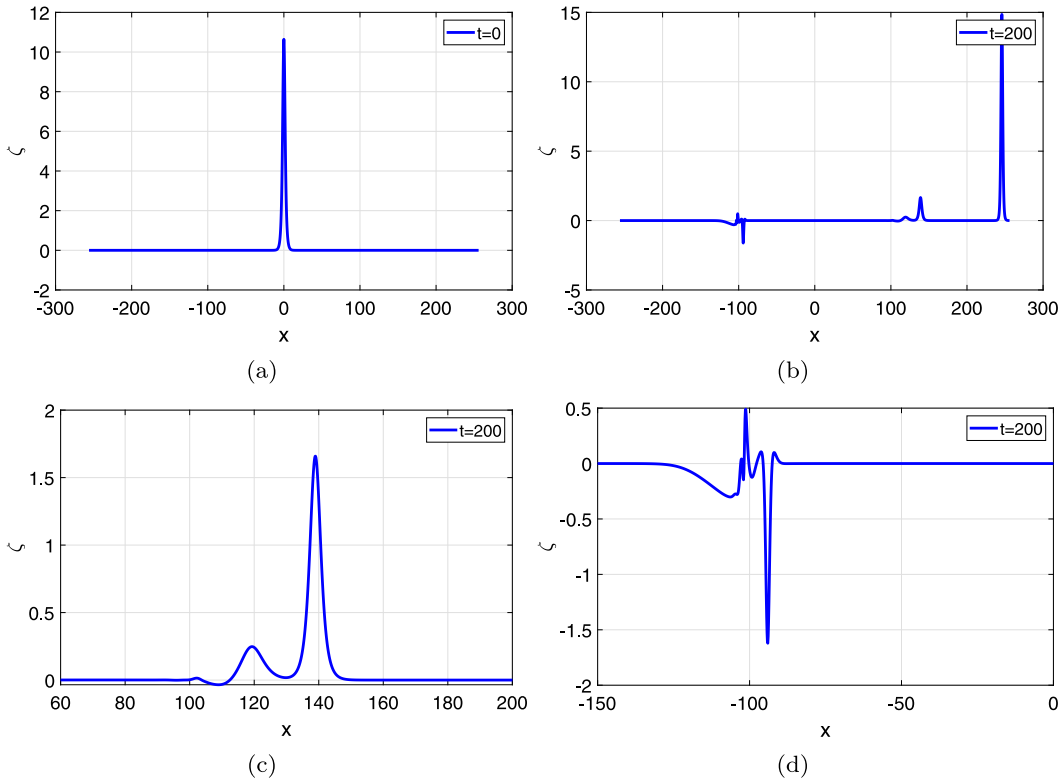

Fig. 12. Evolution of a perturbed CSW. Case (A3) with (3.2), (3.3) $A = 6.1$, $c_s = c_{\gamma,\delta} + 0.1$. (a)–(b) ζ component of the numerical solution; (c) first structure of the ζ component of the numerical solution; (d) second structure.

decreased slightly; the relative difference is 9.7×10^{-6}. In the case of the second, smaller solitary wave, the comparison shows an increase of the amplitude after the collision, which in relative terms is about 2.0×10^{-6}. The effect in the corresponding speeds is qualitatively similar to the experimental speed–amplitude relation shown in Section 2, as the taller wave reduces slightly its speed after the collision, while that of the shorter one is increasing, cf. [2].

Additional features of this inelastic interaction are shown in Figs. 13(c) and 13(d). Behind the shorter emerging wave a small dispersive tail is generated, while a second, wavelet-type structure is observed to have formed and to be traveling to the left.

3.1.4. Head-on collisions

The following experiment on head-on collisions is reported here. With the same parameters as in (3.2), we follow the evolution of the superposition of two approximate CSW-profiles of equal heights, initially centered at $x = \pm 20$, with opposite speeds of absolute values equal to $c_s = c_{\gamma,\delta} + 0.5 \approx 1.0976$. The waves undergo a symmetric head-on collision, shown in Figs. 14(a)–(d).

The outcome of the collision is symmetric as well. After the interaction, there emerge two solitary waves and structures traveling behind them, similar to ones already observed in other experiments. In this case, the amplitude of the emerging right-traveling CSW is smaller than that of the initial one with a relative difference of about 1.8×10^{-3}. The emerging waves are also slightly slower than the initial ones, with a relative decrease of 6.4×10^{-4} in their speeds.

The structures behind the solitary waves, shown in more detail in Figs. 14(c) and 14(d), are of bigger size than those of the previous experiment of overtaking collision, but seem to be again of dispersive and nonlinear type. The form of the nonlinear structure, however, is not yet clear from Fig. 14(d).

Remark 3.2. A second experiment, concerning a non-symmetric head-on collision, was made, cf. [2]. In this case the initial condition is a superposition of two approximate CSW profiles, one with amplitude 11.101, speed $c_s^{(1)} = c_{\gamma,\delta} + 0.5 \approx 1.0976$ (traveling to the right) and centered at $x = -20$, and a second one with amplitude 4.8324, absolute value of speed equal to $c_s^{(2)} = c_{\gamma,\delta} + 0.25 \approx 0.8476$ traveling to the left and centered at $x = 20$. After the non-symmetric interaction, the taller emerging CSW has smaller amplitude than before the collision (with a relative difference of about 6.3×10^{-4}, but the amplitude of the shorter emerging CSW has decreased more (about 5.2×10^{-3}; the corresponding figures can be seen in [2]). Consequently, the emerging CSW's are slower than their corresponding counterparts before the collision. The tails trailing the emerging waves are not symmetric either and they seem to have a similar structure to those of the symmetric head-on collision shown in Fig. 14: A wavelet-type form in front and a strong dispersive component behind.

3.1.5. Resolution property

In addition to the evidence of generation of more than one CSW observed in the evolution of initial profiles with larger perturbations in Section 3.1.2, the resolution into solitary waves also appears in the evolution of other types of initial conditions. This is illustrated in Fig. 15, which represents the temporal behavior of the ζ-component of the numerical solution emerging from an initial Gaussian pulse $\zeta(x, 0) = Ae^{-\tau x^2}$, $u(x, 0) = \zeta(x, 0)$, with $A = 2$, $\tau = 0.01$. In this example, a train of solitary waves of elevation is formed, followed by a left-traveling dispersive structure, see Figs. 15(c) and 15(d). The evolution of the maximum of the ζ-component of the numerical solution stabilizes to around 4.1790, which is the amplitude of the leading solitary wave profile of the train. The speed, computed from the point where the maximum is attained, cf. [47], is about 8.1779×10^{-1}.

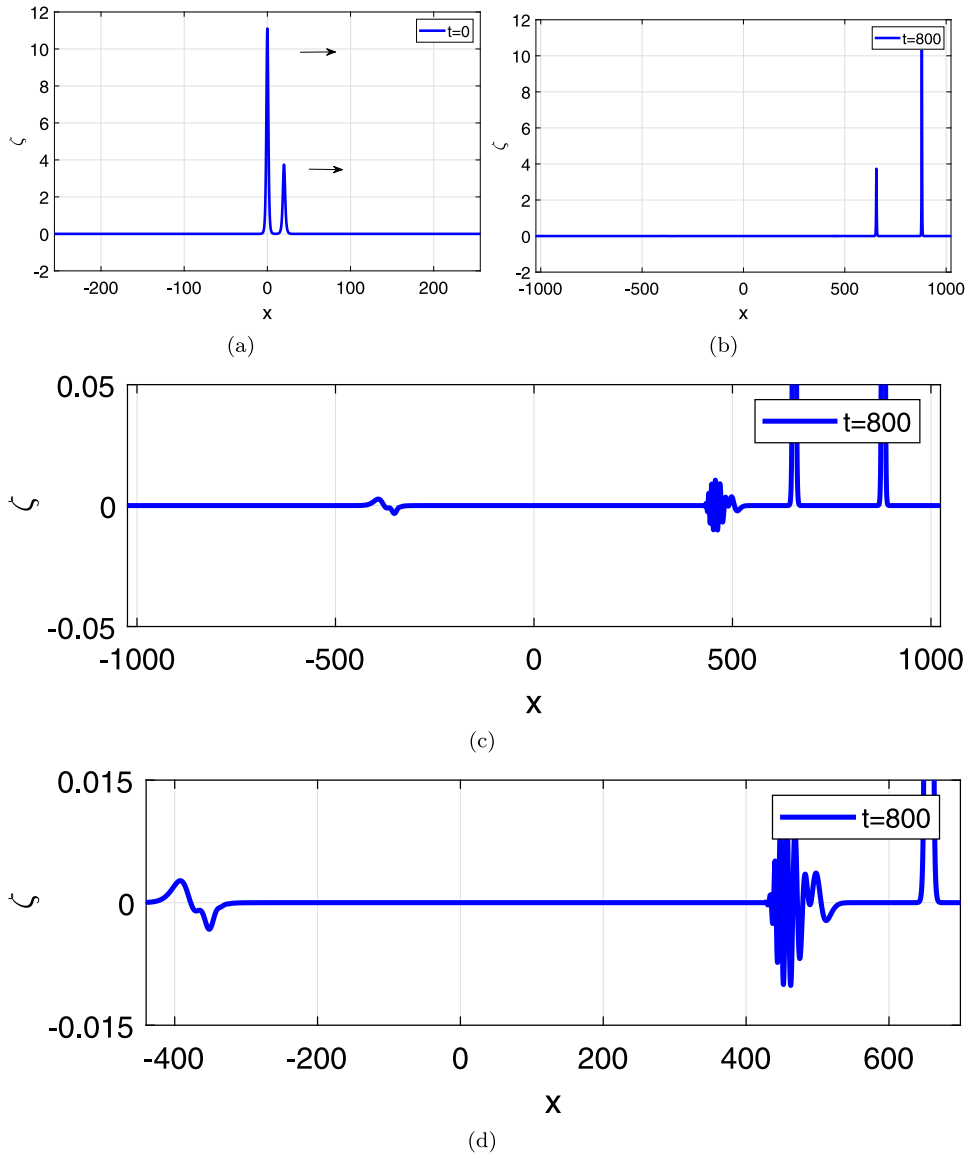

Fig. 13. Overtaking collision of CSW's. (a)–(b) ζ component of the numerical approximation; (c) Magnification of (b); (d) magnification of (c).

3.2. GSW dynamics. Numerical experiments

In this section we illustrate some aspects of the dynamics of GSW's in the generic case (A2) of Table 1. As in the previous section, the experiments are concerned with perturbations and collisions of GSW's.

3.2.1. Perturbations of GSW

We consider the parameters

$$\gamma = 0.5,\ \delta = \frac{\gamma + \sqrt{\gamma^2 + 8}}{2} \approx 1.6861,$$
$$c = -1/6,\ b = 1/9,\ d = 4/3,$$
$$a = \varkappa_1(1/6 - b - c - d) \approx -0.5083, \tag{3.11}$$

and generate the corresponding approximate GSW, with amplitude 4.5728×10^{-2} and speed 4.8824×10^{-1}. (The values of γ and δ in (3.11) are taken appropriately to ensure that the parameters a, b, c and d satisfy the conditions in (A2) in Table 1.) The first experiment consists of perturbing the two components (ζ_s^N, u_s^N) of the GSW with the same quantity $A = 1.01$, i. e. considering

$$\zeta^N(0) = A\zeta_s^N,\ u^N(0) = Au_s^N, \tag{3.12}$$

as initial condition of the numerical method, and monitoring the evolution of the corresponding numerical solution. This is shown in Fig. 16: This small perturbation of the GSW generates a new GSW.

The evolution of the amplitude and speed of the emerging wave suggests that its parameters stabilize at slightly larger values than those of the initial condition. Specifically, the amplitude of the perturbed initial GSW is of about 4.612×10^{-2} and that of emerging GSW is between 4.61×10^{-2} and 4.62×10^{-2}. In the case of the speed, the relative difference is about 3.26×10^{-4}. The structure of the ripples appears to be the same. We expect that the small perturbation will generate some sort of dispersion, for this experiment the dispersive oscillations are apparently of very small size and are probably hidden in the ripples.

The study of the structure of dispersive tails via the linearized system (3.4), (3.5), made in Section 3.1 for the generic case (A3) of classical solitary waves can be adapted to the generic case (A2) for generalized solitary waves (see [2] for the details). Now, for sufficiently large $|k|$, we have

$$-c_s - c_{\gamma,\delta} < v_-(k) < -c_s < v_+(k),$$

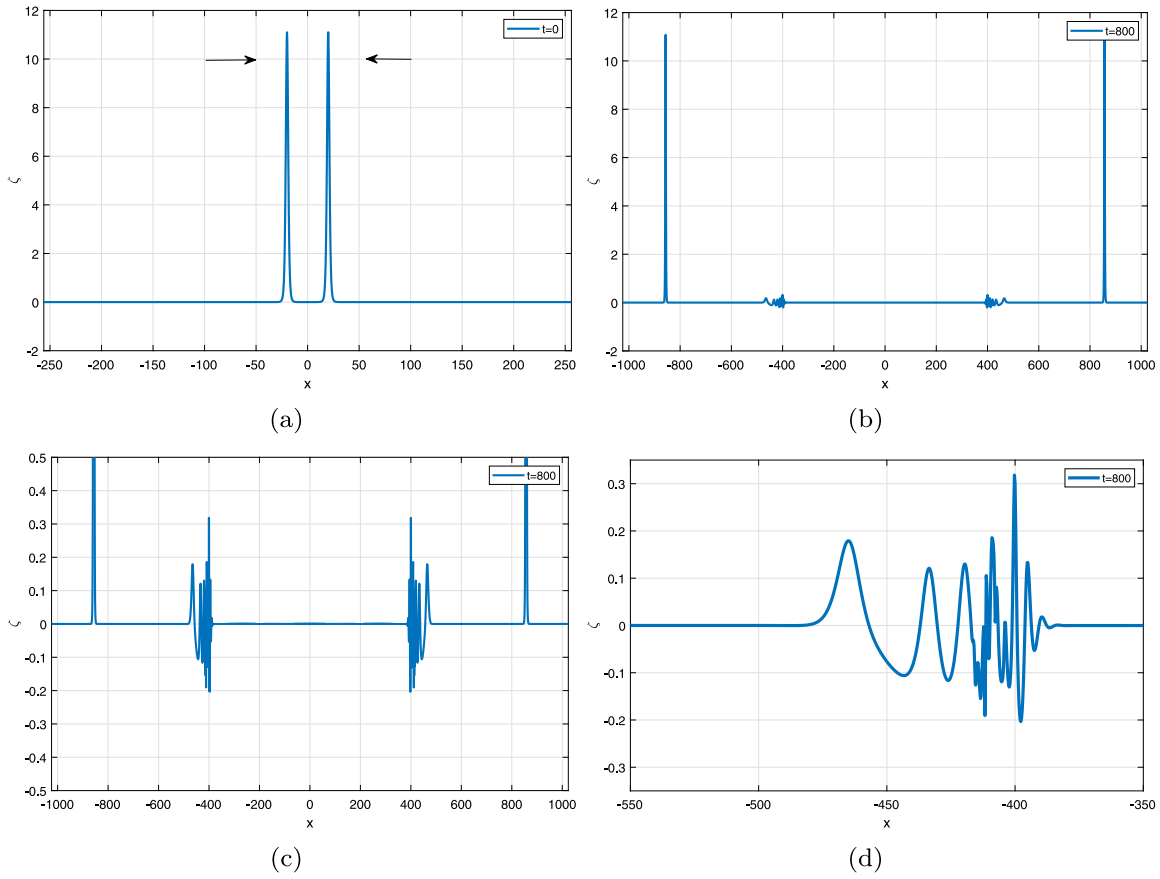

Fig. 14. Symmetric head-on collision of CSW's. (a)–(b) ζ component of the numerical approximation; (c) magnification of (b); (d) magnification of (c) left.

and $v_+(k) > -c_s + c_{\gamma,\delta}$. This implies the existence of plane wave components of small amplitude traveling to the right and in front of the GSW. Similarly, the formation of two dispersive groups, one traveling to the left behind the solitary wave and one to the right in front of it, is suggested by the form of the corresponding function ψ, given by (3.10), for the case (A1).

As the perturbation parameter A grows, new phenomena appear in the dynamics. This is illustrated in Fig. 17, which corresponds to (3.11), (3.12) with $A = 4.1$ (cf. also [2]). The experiment suggests that the perturbed initial GSW evolves into a new GSW which seems to require a longer time to stabilize. Behind the main wave, similar structures to those observed in the case of large perturbations of CSW's (cf. Fig. 11) seem to be generated, superimposed on the ripples. In addition, some perturbation tails radiate in front of the main emerging wave. This fact and the longer time required for the stabilization of the main wave may suggest some kind of instability.

3.2.2. Resolution

In order to study the resolution property in systems with generalized solitary wave solutions, we consider again the values of the parameters given by (3.11) and use, as initial condition, the same Gaussian pulse as that considered in Section 3.1 for CSW's, of the form $\zeta(x,0) = Ae^{-\tau x^2}$, with $A = 2$, $\tau = 0.01$, and $u(x,0) = \zeta(x,0)$. The evolution of the numerical approximation is illustrated in Fig. 18.

The behavior of the approximation of ζ may be compared with that of the CSW case (Fig. 15). Now, the Gaussian profile seems to evolve into a train of solitary waves of elevation, followed by some structures of different form. They are displayed in more detail in Fig. 19. Fig. 19(a) is a magnification of the tail formed just behind the solitary wave train and Fig. 19(b) is a detail of the solution between two solitary waves. Some dispersive pulses are radiated in front of each profile. These are also observed behind the wave train of solitary waves, see Fig. 19(c). A third structure, magnified in Fig. 19(d), seems to consist of a train of classical solitary waves with non-monotonic decay and a dispersive tail.

3.2.3. Head-on collisions

The interactions of GSW's are illustrated with experiments of head-on collisions. The first experiment shown in the sequel is concerned with a symmetric head-on collision of GSW's. For the system with parameters given by (3.11), a superposition of approximate GSW profiles with absolute values of the speed $c_s = c_{\gamma,\delta} + 10^{-2} \approx 4.8824 \times 10^{-1}$, traveling to the right and to the left and centered at $x_0 = -20$ and $x_0 = 20$ respectively, is taken as initial condition, and the simulation of the evolution is represented in Fig. 20. The initial amplitudes are about 4.5654×10^{-2}.

The temporal interval of collision lasts approximately from $t = 30$ to $t = 50$; thereafter two symmetric GSW's emerge. The evolution of the amplitude of the ζ component of the numerical solution seems to stabilize to a value around 4.62×10^{-2}; so the emerging waves are taller (and hence faster), and the relative difference in amplitude is about 1.2×10^{-2}. We note that after the collision the amplitude of the ripples is larger.

From the experiments (not presented here, cf. [2]) to illustrate the dynamics of non-symmetric head-on collisions, similar effects to those of the symmetric collision case are observed.

3.3. Dynamics of classical solitary wave solutions with non monotone decay

In this section we present some experiments concerning the dynamics of CSW solutions of (1.1) with non monotone decay,

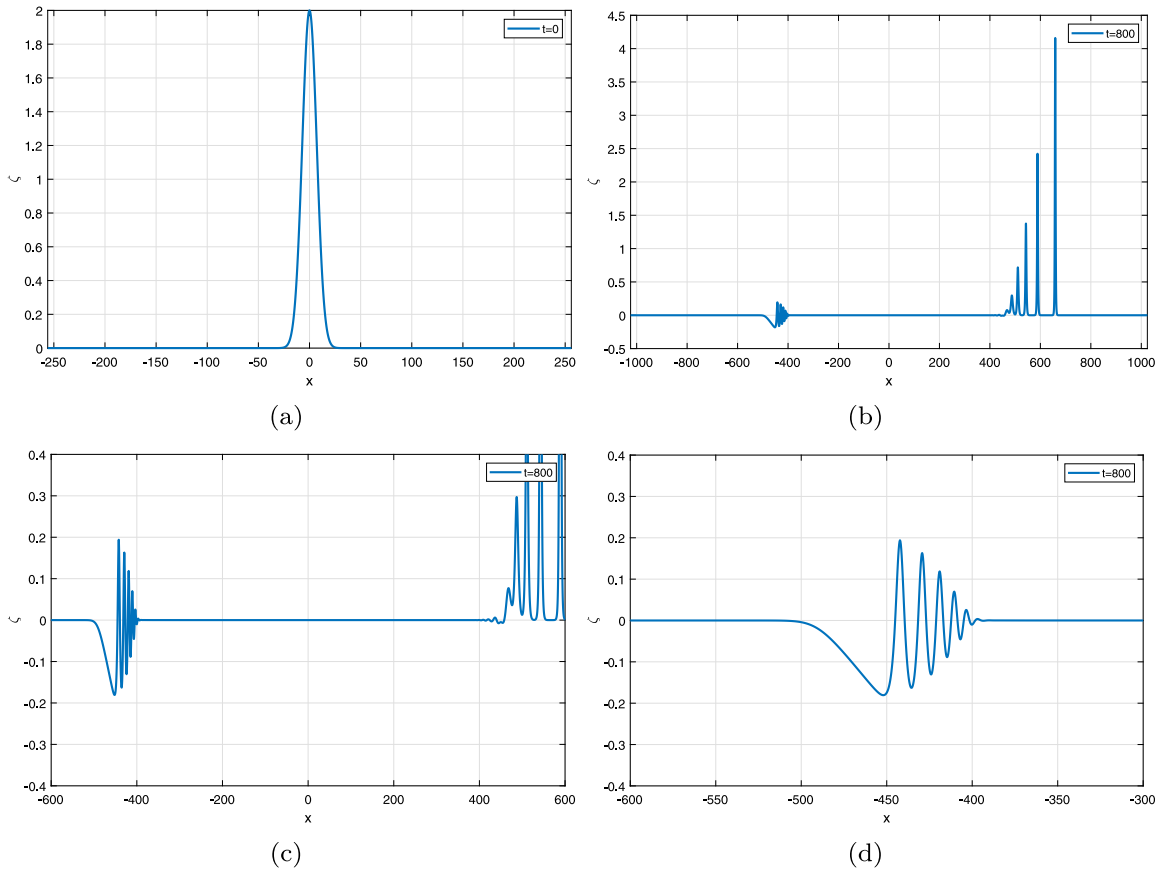

Fig. 15. Resolution property. Initial Gaussian pulse $\zeta(x,0) = Ae^{-\tau x^2}$, $u(x,0) = \zeta(x,0)$, with $A = 2$, $\tau = 0.01$. Case (A3). (a)–(b) ζ component of the numerical solution; (c) magnification of (b); (d) magnification of (c).

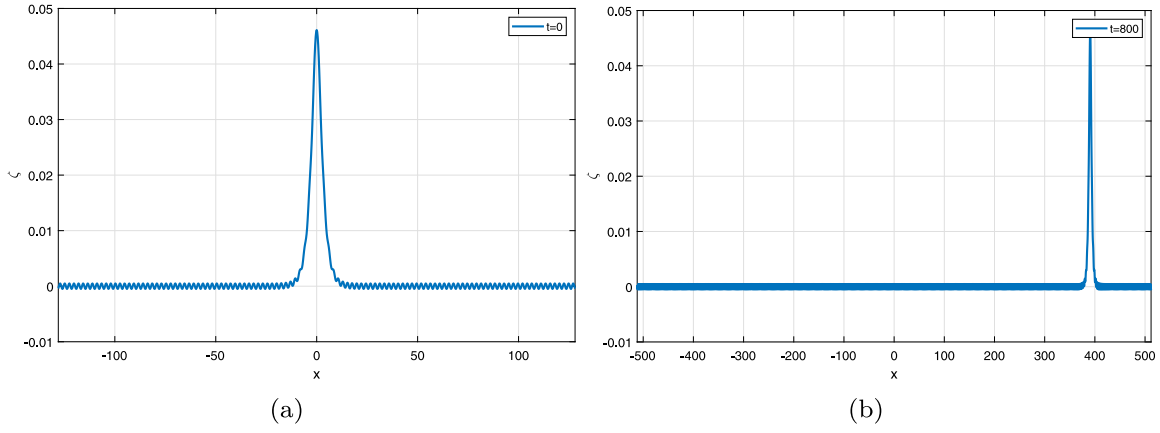

Fig. 16. Small perturbation of a GSW. Case (A2) with (3.11), (3.12) with $A = 1.01$. (a) Perturbed GSW profile; (b) ζ component of the numerical solution.

whose existence was justified by an application of the Normal Form Theory in Section 2.1, and for speeds smaller than the corresponding speed of sound $c_{\gamma,\delta}$. For simplicity we focus on the behavior under small and large perturbations of the type (3.12) as those used in Sections 3.1 and 3.2 .

We consider the numerical profile obtained in Section 2.2 from the parameters

$$\gamma = 0.5, \delta = 0.9,$$
$$a = -1/9, b = 0, c = -1/6,$$
$$d = S(\gamma,\delta) - \frac{a}{\varkappa_1} - b - c \approx 0.7058. \tag{3.13}$$

The ζ component has a maximum negative excursion of about -2.8740 and the speed is $c_s = c_{\gamma,\delta} - 0.2 \approx 0.3976$. The ζ_h and v_h components are perturbed in amplitude with a perturbation factor $A = 1.1$. The perturbed wave $(A\zeta_h, Av_h)$ is taken as initial condition of the numerical method to approximate (1.1) with $L = 1024$, and the evolution of the resulting numerical approximation is monitored up to $t = 800$ and shown in Fig. 21.

During the evolution, a new solitary wave of the same type is formed. Compared to the initial perturbed wave, whose maximum negative excursion was approximately -3.1614, the emerging wave dips to about -3.1376. The wave is slower, with a speed around 0.3832.

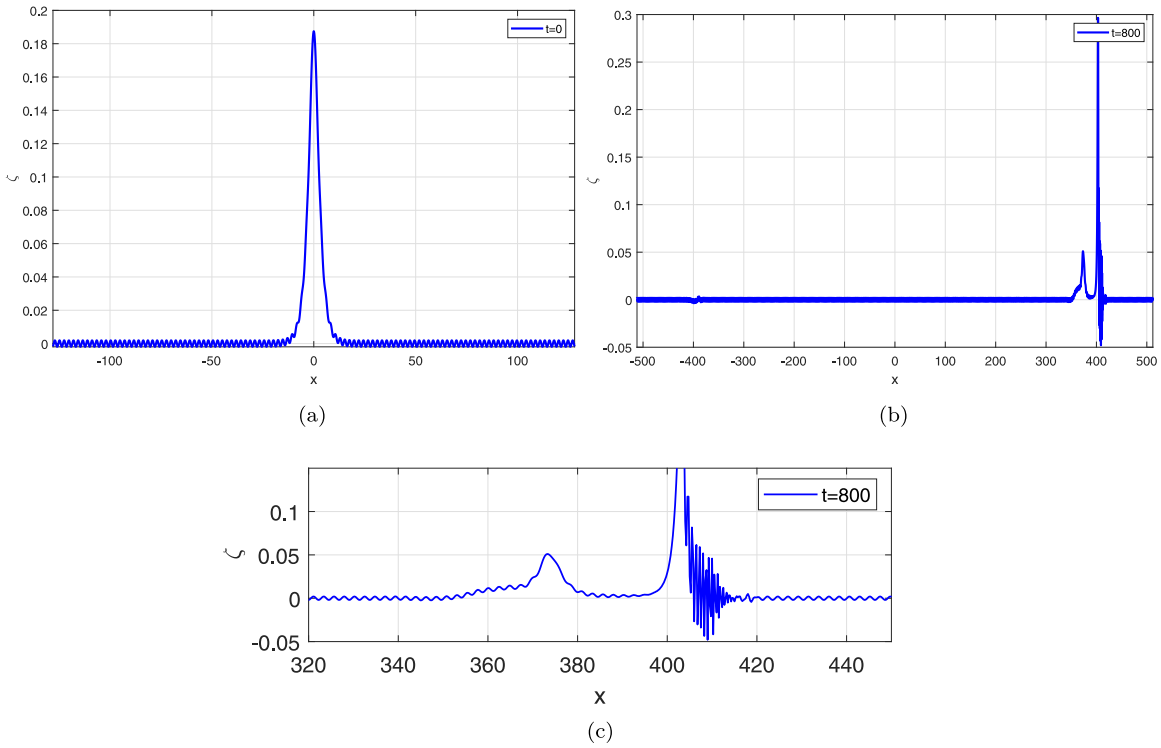

Fig. 17. Large perturbation of a GSW. Case (A2) with (3.11), (3.12) with $A = 4.1$. (a) Perturbed GSW profile; (b) ζ component of the numerical solution; (c) magnification of (b).

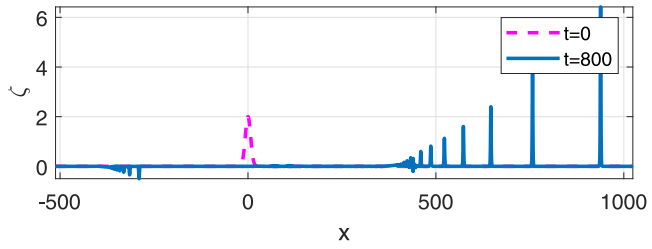

Fig. 18. Resolution property. Case (A2) with (3.11), and a Gaussian pulse $\zeta(x,0) = u(x,0) = Ae^{-\tau x^2}$, with $A = 2$, $\tau = 0.01$, as initial condition. ζ component of the numerical solution.

Behind and in front of the emerging solitary wave, some other small structures form. They are observed in the magnification of Fig. 21(b) given by Fig. 21(c) and (d).

The main character of these small-amplitude waves seems to be dispersive. The generation of dispersive oscillations in front of the emerging solitary wave can be justified from the study of small-amplitude solutions of the linearized system (3.4), (3.5). In this case we have a linear dispersion relation of the form

$$\omega(k) = \omega_{\pm}(k) = -kc_s \pm c_{\gamma,\delta} k\phi(k^2),$$

where $\phi : [0,\infty) \to \mathbb{R}$ is the function

$$\phi(x) = \sqrt{\frac{(1-\widetilde{a}x)(1-cx)}{1+dx}}, \quad \widetilde{a} = \frac{a}{\varkappa_1},$$

with a, c, d given by (3.13). The local phase speed (relative to the speed of the CSW) is therefore

$$v_{\pm}(k) = -c_s \pm c_{\gamma,\delta}\phi(k^2).$$

An analysis of ϕ similar to that made in Section 3.2 for the case (A1) shows that for large $|k|$

$$v_{+}(k) > -c_s + c_{\gamma,\delta},$$

and most of the components of the dispersive tail travel to the right and in front of the solitary wave. Similarly, for the group velocities

$$\omega'_{\pm}(k) = -c_s \pm c_{\gamma,\delta}\psi(k^2),$$

where $\psi : [0,\infty) \to \mathbb{R}$ is given by (3.10), and for $|k|$ large enough

$$\omega'_{+}(k) \geqslant -c_s + c_{\gamma,\delta} > 0.$$

Hence one dispersive group travels to the right and in front of the solitary wave.

We repeat now the analogous experiment with $A = 2.1$ in (3.12), and the results are shown in Fig. 22. As the perturbation factor A grows, the size of both tails also grows. In addition, Figs. 22(c) and 22(d) suggest the formation of nonlinear structures, in the form of wavelets and perhaps some very small CSW's with non monotone decay. (These two structures were conjectured in Fig. 21(d).) The emerging solitary wave is shorter (its maximum negative excursion is approximately -5.233, compared to -6.035 for the initial perturbed wave) and slower (the speed is now about 0.237).

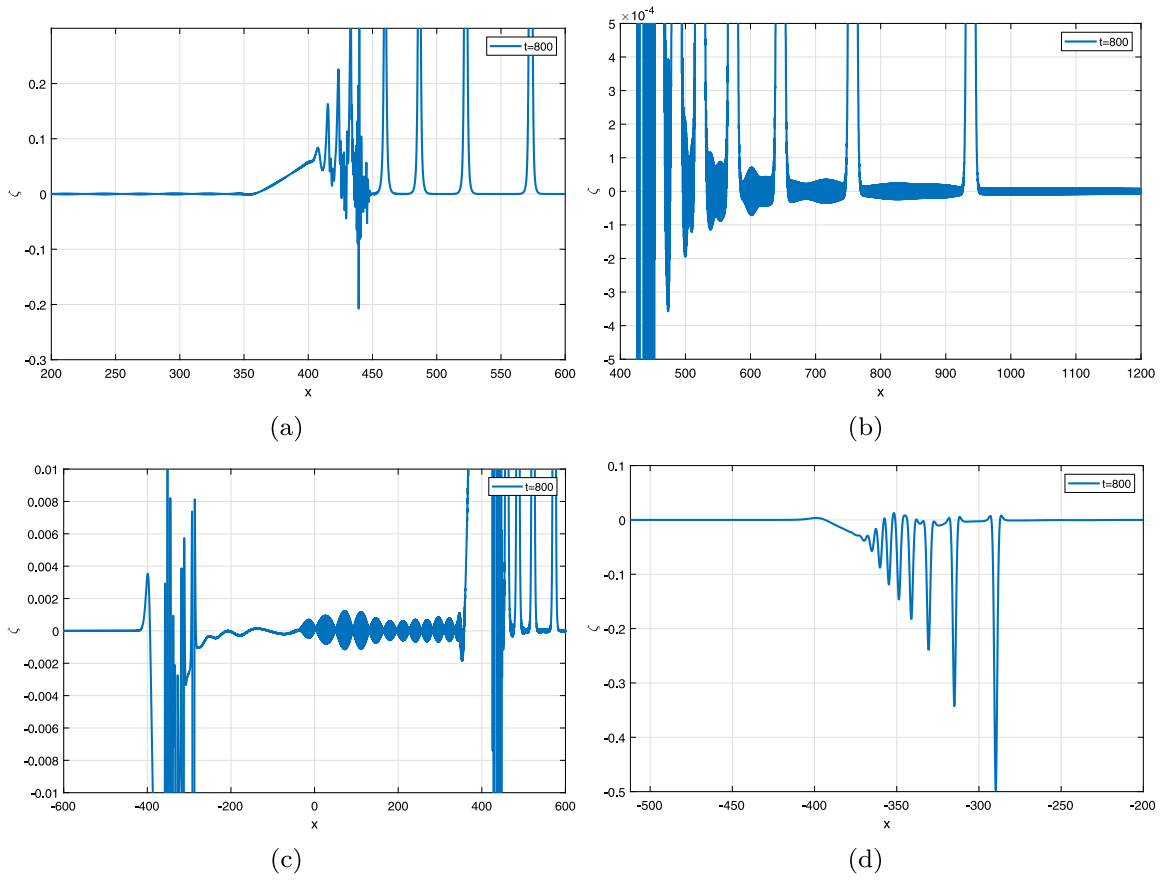

Fig. 19. Resolution property. Case (A2) with (3.11), and a Gaussian pulse $\zeta(x,0) = u(x,0) = Ae^{-\tau x^2}$, with $A = 2$, $\tau = 0.01$, as initial condition. Several structures of the ζ component of the numerical solution at $t = 800$.

4. Concluding remarks

The present paper continues the study, initiated in [1], of the so-called Boussinesq/Boussinesq (B/B) systems (1.1). They model the propagation of the deviation of the interface in a two-layer system of fluids, with the upper layer bounded above by a horizontal rigid lid and the lower layer bounded below by an impermeable, horizontal bottom, under a Boussinesq regime for the flow in both layers, [3]. In [1], some theoretical results of the ivp for (1.1), concerning linear and nonlinear well-posedness, Hamiltonian structure, and conservation laws were established. In addition, and for each nonlinearly well posed system, error estimates for the spectral Fourier–Galerkin semidiscretization to approximate the corresponding periodic ivp were derived in that paper. We also introduced a full discretization by integrating in time the spectral semidiscrete systems with a fourth-order RK method of composition type based on the implicit midpoint rule.

The present paper is focused on the existence and dynamics of solitary-wave solutions of the B/B systems. Section 2 is concerned with the existence and numerical generation of this type of solutions. In the first part, Section 2.1, we apply standard theories such as Normal Form Theory (NFT), Toland's Theory, Concentration–Compactness Theory (CCT), and Positive Operator Theory (POT), in order to derive existence results. If we make use of the linearization of the system for the solitary waves (2.1), written as a first-order system (2.3), at the origin, NFT allows us to establish the existence of Classical Solitary Waves (CSW's) and Generalized Solitary Waves (GSW's), in two 'generic' cases (cf. Table 1), respectively:

- $a, c \leqslant 0, b, d \geqslant 0, bd - ac/\varkappa_1 > 0$ (CSW),
- $a, c \leqslant 0, b, d \geqslant 0, bd - ac/\varkappa_1 < 0$ (GSW),

where $\varkappa_1 = 1/(\delta + \gamma)$, with δ and γ denoting, respectively, the depth and density ratios of the two-layer system of fluids. Existence of such solitary waves is ensured by the NFT when the magnitude of the speed c_s is greater than but close to the limiting value $c_{\gamma,\delta} = \sqrt{(1-\gamma)/(\delta+\gamma)}$ (speed of sound). In addition, NFT also predicts periodic solutions close to the region of generation of CSW's, as well as classical solitary waves with non monotone decay for speeds c_s satisfying $|c_s| < c_{\gamma,\delta}$.

The remaining theories contribute more results for the existence of CSW's of speeds not necessarily close to $c_{\gamma,\delta}$. Thus:

- When $a, c \leqslant 0, b = d > 0$ (Hamiltonian case), Toland's theory ensures the existence of classical solitary waves. A specific speed–amplitude relation of the form (2.21) holds.
- When $a, c < 0, b = d > 0$, CCT establishes the existence of CSW's for speeds c_s satisfying a bound of the form (2.26) and $|c_s| < c_{\gamma,\delta}$.
- The application of POT proves the existence of CSW's when $b, d > 0, a, c \leqslant 0$, and $bd - ac/\varkappa_1 > 0$, with speeds c_s satisfying $|c_s| > c_{\gamma,\delta}$.

These existence results are illustrated in Section 2.2, where CSW and GSW solutions are numerically generated. The numerical procedure consists of discretizing the system (2.1) of ode's satisfied by the solitary wave profiles, on a long enough interval with periodic boundary conditions, by the Fourier collocation method. In the Fourier space, the differential equation systems for the profiles become algebraic systems, which are iteratively solved by Petviashvili's scheme, accelerated with vector extrapolation techniques. Each case is illustrated by exhibiting the approximate solitary-wave profiles (ζ and v_β components) and the

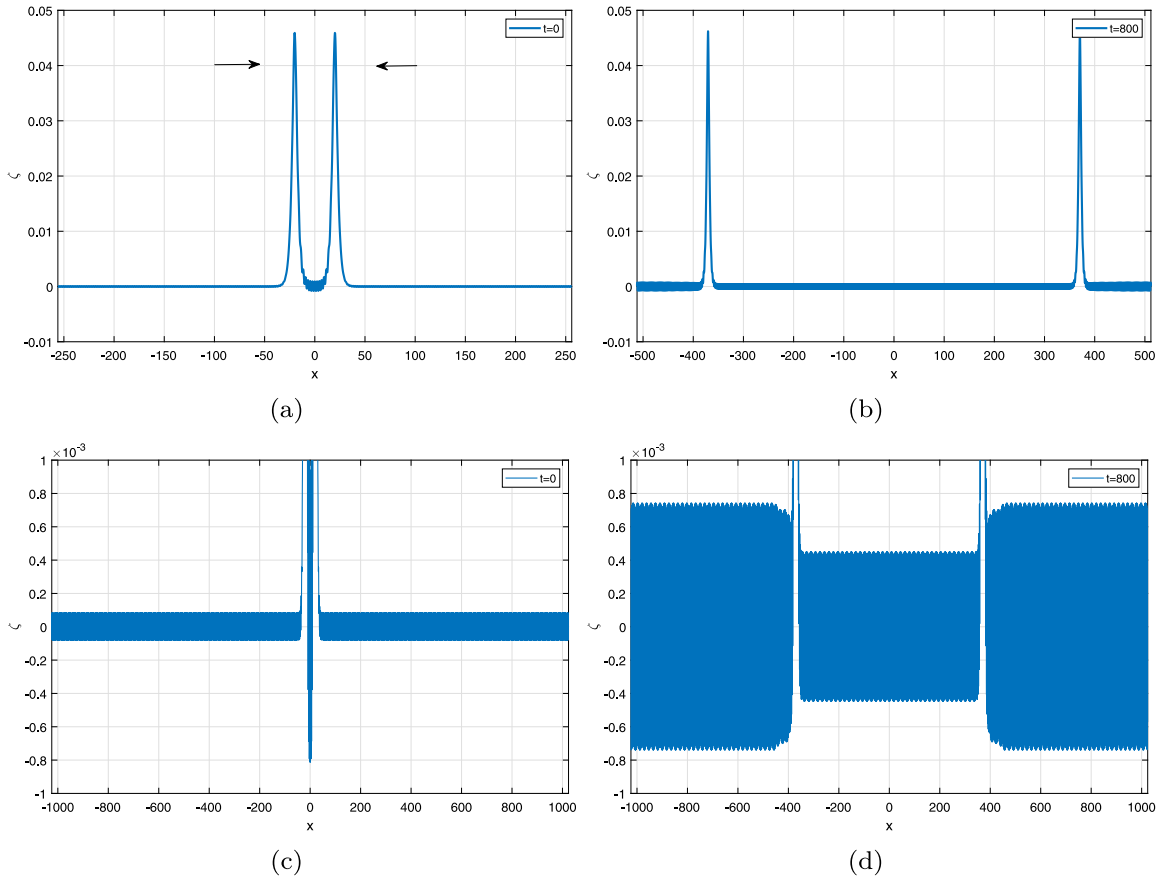

Fig. 20. Symmetric head-on collision of GSW's. Case (A2) with (3.11). (a), (b) ζ component of the numerical solution; (c), (d) magnifications of (a) and (b) respectively.

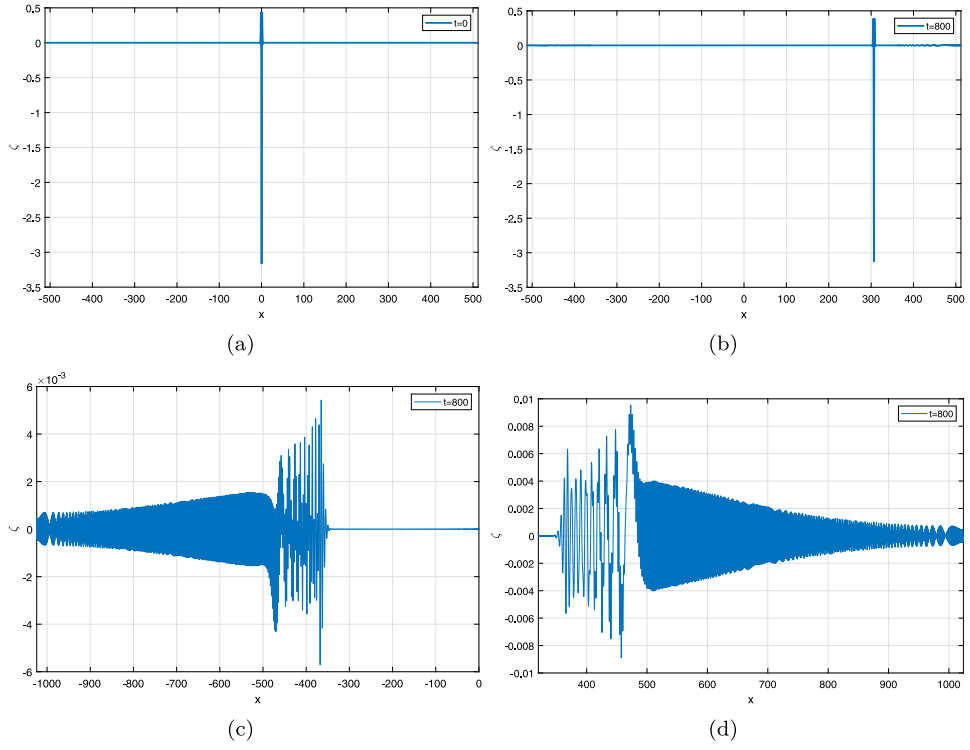

Fig. 21. Small perturbation of a CSW with nonmonotone decay. $A = 1.1$. (a), (b) ζ component of the numerical solution; (c), (d) magnifications of (b).

corresponding phase portraits, while the decrease of the residual error with the number of iterations was checked in order to verify the convergence of the iteration. In addition, numerical experiments suggest in all cases, and for both CSW's and GSW's, that

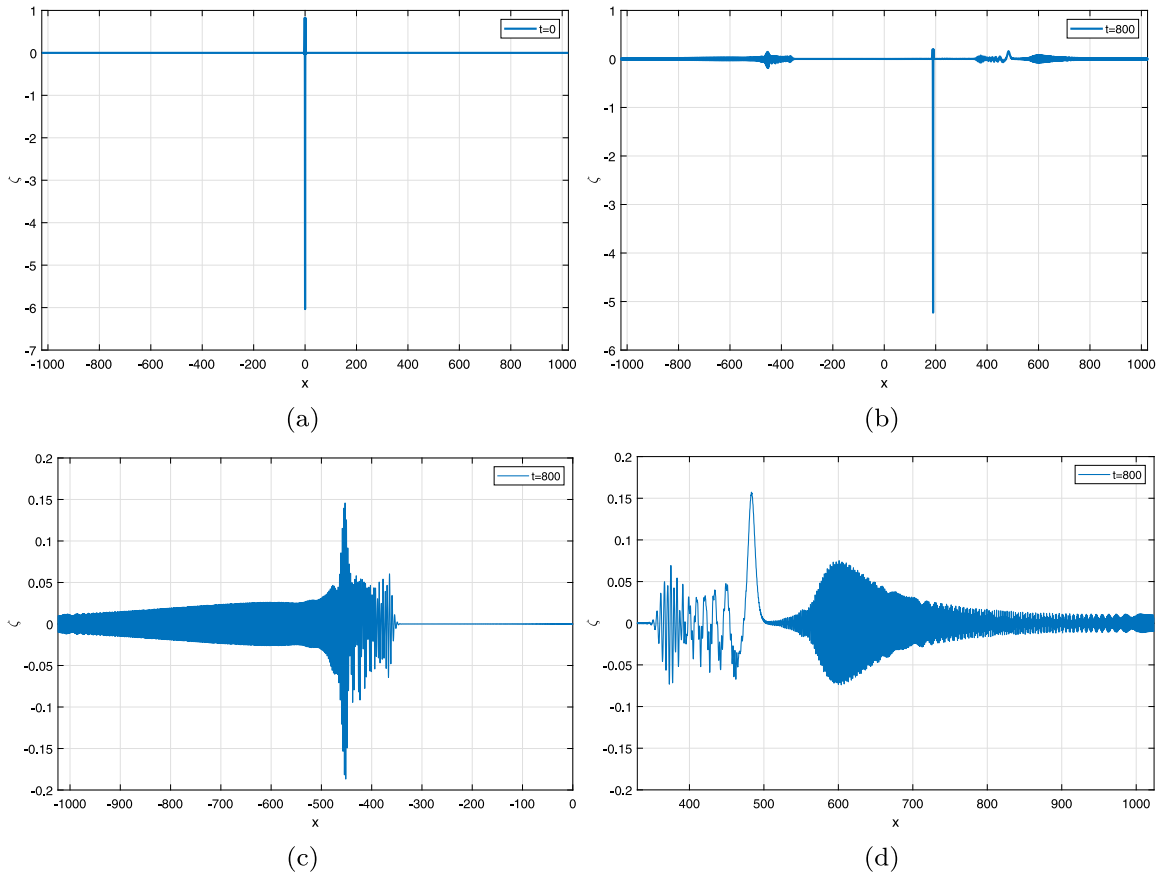

Fig. 22. Perturbation of a CSW with nonmonotone decay. $A = 2.1$. (a), (b) ζ component of the numerical solution; (c), (d) magnifications of (b).

the amplitude is an increasing function of the speed difference $c_s - c_{\gamma,\delta}$.

In Section 3 we make a computational study of some aspects of the dynamics of classical and generalized solitary waves of the B/B systems by solving numerically the periodic ivp on a long enough interval using the fully discrete method presented in [1]. Section 3.1 is devoted to a computational study of the dynamics of CSW solutions which are strictly positive or negative. The experiments are made for the generic case $a, c < 0, b, d > 0, bd - ac/\varkappa_1 > 0$ and describe the ensuing evolution from small and large perturbations of CSW's, from superpositions of CSW's (in order to study overtaking and head-on collisions), and from Gaussian pulses, in order to study resolution into solitary waves. Some of the main conclusions are reported here:

- Under small initial perturbations, the solution evolves into a modified CSW with small dispersive tails following the main wave. The generation and structure of these tails are justified by an analysis of small-amplitude solutions of the associated linearized system in a reference frame moving with the speed of the solitary wave. In the case of these strictly positive or negative classical solitary waves, the results predict the formation of two types of dispersive oscillation groups, trailing the solitary wave and traveling in opposite directions.
- Increasing the size of the perturbation of the initial solitary wave may lead to the generation of additional stable, nonlinear structures. They may consist of smaller CSW's, CSW's of non monotone decay or others of wavelet type.
- The collisions are, as expected, inelastic. In both cases (overtaking and head-on collisions), two CSW's emerge; the effects of the inelastic interactions include the generation of tails of dispersive nature and nonlinear structures of the same type as those already mentioned.
- The evolution ensuing from initial Gaussian pulses shows resolution into a train of CSW's, leaving a small structure behind which seems to be dispersive.

In Section 3.2 we carry out a corresponding computational study of the dynamics of GSW's. The experiments concern systems in the generic case $a, c < 0, b, d > 0, bd - ac/\varkappa_1 < 0$ and are of the same type as those in Section 3.1. The main conclusions are:

- The experiments with small perturbations of GSW's suggest that the question of stability of these waves is more intricate, in the sense that the formation of emerging, stable GSW's seems to require smaller initial perturbations and takes longer time than in the case of CSW's. In some examples the dispersive tails are hard to observe, as they are hidden in the ripples of the structure, being of much smaller size.
- The experiments with larger perturbations of an initial GSW show the formation of nonlinear structures of similar type to those observed in the case of CSW's, but overimposed on the ripples. In addition, larger ripples along with dispersive tails form in front of an emerging GSW, a fact that surely affects its stability.
- The experiments show the evolution, from initial Gaussian pulses, of a train of solitary-wave type pulses traveling to the right. Ripples are formed between each pair of consecutive pulses, mixed somehow with dispersive tails. These dispersive groups are also observed behind the train. Finally, a second train of solitary-wave pulses is formed, traveling to the left, consisting of nonmonotonically decaying solitary

waves; thus each wave of this train should have speed less than the limiting value $c_{\gamma,\delta}$.

- The main effect observed in the experiments of overtaking and head-on collisions of GSW's is the formation of two emerging GSW's with ripples of different size, larger, in general, than those of the initial GSW's. Dispersive structures seem now to be smaller and are superimposed on the emerging ripples.

The existence of nonmonotonically decaying classical solitary waves, established in Section 2.1 and numerically generated in Section 2.2, as well as their role in the dynamics of other solitary waves, observed in the experiments of Sections 3.1 and 3.2, motivate the numerical experiments of Section 3.3, devoted to a computational study of the behavior of these waves under small and large perturbations. The experiments suggest persistence and stability of these waves. From small perturbations, a new solitary wave of the same type is formed. The analysis of small-amplitude plane wave solutions of the linearized system in a reference moving with the speed of the solitary wave, shows now that the main part of the dispersive oscillations travels to the right in front of the solitary wave, with the rest traveling to the left, behind it. When the perturbation factor grows, the formation of a new solitary wave with nonmonotone decay is observed, and now the dispersive tails seem to be accompanied by the generation of small nonlinear structures, in the form of wavelets or nonmonotone CSW's.

CRediT authorship contribution statement

Vassilios A. Dougalis: Conceptualization, Methodology, Investigation, Supervision, Writing – original draft, Writing – review & editing. **Angel Durán:** Conceptualization, Methodology, Investigation, Supervision, Writing – original draft, Writing – review & editing. **Leetha Saridaki:** Conceptualization, Methodology, Investigation, Supervision, Writing – original draft, Writing – review & editing.

Declaration of competing interest

The authors declare that they have no known competing financial interests or personal relationships that could have appeared to influence the work reported in this paper.

Acknowledgments

The authors are supported by the Spanish Ministerio de Ciencia e Innovación under Research Grant PID2020-113554GB-100. They would like to acknowledge travel support, that made possible this collaboration, from the Institute of Applied and Computational Mathematics of FORTH and the Institute of Mathematics (IMUVA) of the University of Valladolid. Angel Durán is also supported by the Junta de Castilla y León and the EU (European Regional Development Fund) under Research Grant VA193P20. Leetha Saridaki is also supported by the grant "Innovative Actions in Environmental Research and Development (PErAn)" (MIS5002358), implemented under the "Action for the strategic development of the Research and Technological sector" funded by the Operational Program "Competitiveness, and Innovation" (NSRF 2014-2020) and co-financed by Greece and the EU (European Regional Development Fund). The grant was issued to the Institute of Applied and Computational Mathematics of FORTH.

References

[1] V.A. Dougalis, A. Durán, L. Saridaki, On the numerical approximation of Boussinesq/Boussinesq systems for internal waves, in press.
[2] V.A. Dougalis, A. Durán, L. Saridaki, Notes on the numerical analysis and solitary wave solutions of Boussinesq/Boussinesq systems for internal waves, Preprint available at http://arxiv.org/abs/2012.07992.
[3] J.L. Bona, D. Lannes, J.C. Saut, Asymptotic models for internal waves, J. Math. Pures Appl. 89 (2008) 538–566.
[4] J.-C. Saut, Asymptotic models for surface and internal waves, in: 29^{O} Colóquio Brasileiro de Matemática, IMPA, Rio de Janeiro, 2013.
[5] J.L. Bona, M. Chen, J.-C. Saut, Boussinesq equations and other systems for small-amplitude long waves in nonlinear dispersive media: I. Derivation and linear theory, J. Nonlinear Sci. 12 (2002) 283–318.
[6] J.L. Bona, M. Chen, J.-C. Saut, Boussinesq equations and other systems for small-amplitude long waves in nonlinear dispersive media: II. The nonlinear theory, Nonlinearity 17 (2004) 925–952.
[7] C.T. Anh, On the Boussinesq/Full dispersion systems and Boussinesq/Boussinesq systems for internal waves, Nonlinear Anal. 72 (2010) 409–429.
[8] C. Burtea, New long time existence results for a class of Boussinesq-type systems, J. Math. Pures Appl. 106 (2) (2016) 203–236.
[9] J.C. Saut, L. Xu, The Cauchy problem on large time for surface waves Boussinesq systems, J. Math. Appl. (9) 97 (6) (2012) 635–662.
[10] J.C. Saut, C. Wang, L. Xu, The Cauchy problem on large time for surface waves Boussinesq systems II, SIAM J. Math. Anal. 49 (4) (2017) 2321–2386.
[11] C. Kwak, C. Muñoz, F. Poblete, J.C. Pozo, The scattering problem for Hamiltonian ABCD Boussinesq systems in the energy space, J. Afr. Math. Pures Appl. 127 (2019) 121–159.
[12] C. Kwak, C. Muñoz, Asymptotic dynamics for the small data weakly dispersive one-dimensional Hamiltonian abcd systems, Trans. Amer. Math. Soc. 373 (2) (2020) 1043–1107.
[13] H. Yoshida, Construction of higher order symplectic integrators, Phys. Lett. A 150 (1990) 262–268.
[14] J. de Frutos, J.M. Sanz-Serna, An easily implementable fourth-order method for the time integration of wave problems, J. Comput. Phys. 103 (1992) 160–168.
[15] V.A. Dougalis, A. Durán, Notes on a high order fully discrete scheme for the Korteweg–de Vries equation with a time stepping procedure of Runge–Kutta Composition type, in press. Preprint available at: http://arxiv.org/abs/2005.12955.
[16] G. Iooss, M. Adelmeyer, Topics in Bifurcation Theory and Applications, second ed., World Scientific, Singapore, 1999.
[17] M. Haragus, G. Iooss, Local Bifurcations, Center Manifolds, and Normal Forms in Infinite-Dimensional Dynamical Systems, Springer, London, Dordrecht, Heidelberg, New York, 2011.
[18] J.F. Toland, Existence of symmetric homoclinic orbits for systems of Euler–Lagrange equations, in: A. M. S. Proceedings of Symposia in Pure Mathematics, 45(2) 1986, pp. 447–459.
[19] P.L. Lions, The concentration-compactness principle in the calculus of variations. The locally compact case. Part I and Part II, Ann. Inst. Henri Poincare A 1 (1984) 109–145, 223-283.
[20] T.B. Benjamin, J.L. Bona, D.K. Bose, Solitary-wave solutions of nonlinear problems, Philos. Trans. R. Soc. Lond. Ser. A Math. Phys. Eng. Sci. 331 (1990) 195–244.
[21] V.I. Petviashvili, Equation of an extraordinary soliton, Sov. J. Plasma Phys. 2 (1976) 257–258.
[22] D.E. Pelinovsky, Y.A. Stepanyants, Convergence of Petviashvili's iteration method for numerical approximation of stationary solutions of nonlinear wave equations, SIAM J. Numer. Anal. 42 (2004) 1110–1127.
[23] A. Sidi, Vector Extrapolation Methods with Applications, SIAM Philadelphia, 2017.
[24] H.Y. Nguyen, F. Dias, A Boussinesq system for two-way propagation of interfacial waves, Physica D 237 (2008) 2365–2389.
[25] V. Duchêne, Boussinesq-Boussinesq systems for internal waves with a free surface and the KdV approximation, ESAIM Math. Model. Numer. Anal. 46 (2012) 145–185.
[26] J.L. Bona, V.A. Dougalis, D.E. Mitsotakis, Numerical solution of KdV-KdV systems of Boussinesq equations: I. The numerical scheme and generalized solitary waves, Math. Comput. Simulation 74 (2007) 214–228.
[27] V.A. Dougalis, D.E. Mitsotakis, Theory and numerical analysis of Boussinesq systems: A review, in: N.A. Kamparis, V.A. Dougalis, J.A. Ekaterinaris (Eds.), Effective Computational Methods in Wave Propagation, CRC Press, 2008, pp. 63–110.
[28] G. Iooss, K. Kirchgässner, Water waves for small surface tension: An approach via normal form, Proc. Roy. Soc. Edinburgh Sect. A 112 (1992) 200–267.
[29] A.R. Champneys, Homoclinic orbits in reversible systems and their applications in mechanics, fluids and optics, Physica D 112 (1998) 158–186.

[30] E. Lombardi, Oscillatory Integrals and Phenomena beyond All Algebraic Orders, Springer-Verlag, Berlin, Heidelberg, 2000.
[31] G. Iooss, M.C. Peroueme, Perturbed homoclinic solutions in reversible 1 : 1 resonance vector fields, J. Differential Equations 102 (1993) 62–88.
[32] A.R. Champneys, J.F. Toland, Bifurcation of a plethora of multi-modal homoclinic orbits for autonomous Hamiltonian systems, Nonlinearity 6 (1993) 665–772.
[33] L.A. Belyakov, Bifurcation of systems with homoclinic curve of a saddle-focus with saddle quantity zero, Mat. Zametki 36 (1984) 838–843.
[34] R.L. Devaney, Homoclinic orbits in Hamiltonian systems, J. Differential Equations 21 (1976) 431–438.
[35] A. Durán, On a nonlocal Boussinesq system for internal wave propagation, in: J.L. García Guirao, J.A. Murillo, F. Periago (Eds.), Recent Advances in Differential Equations and Applications, Springer, 2019.
[36] D.C. Antonopoulos, V.A. Dougalis, Numerical solution of the 'classical' Boussinesq system, Math. Comput. Simulation 82 (2012) 984–1007.
[37] M. Chen, Exact traveling-wave solutions to bi-directional wave equations, Internat. J. Theoret. Phys. 37 (1998) 1547–1567.
[38] M. Chen, Solitary-wave and multi pulsed traveling-wave solutions of Boussinesq systems, Appl. Anal. 75 (2000) 213–240.
[39] J. Angulo-Pava, Nonlinear dispersive equations, in: Existence and Stability of Solitary and Periodic Travelling Wave Solutions, Amer. Math. Soc., Providence, Rhode Island, 2009.
[40] E.S. Bao, R.M. Chen, Q. Liu, Existence and symmetry of ground states to the Boussinesq abcd systems, Arch. Ration. Mech. Anal. 216 (2015) 569–591.
[41] J. Angulo-Pava, J.-C. Saut, Existence of solitary wave solutions for internal waves in two-layer systems, Quart. Appl. Math. 78 (2020) 75–105.
[42] J.L. Bona, H. Chen, Solitary waves in nonlinear dispersive systems, Discrete Contin. Dyn. Syst. Ser. B 2 (3) (2002) 313–378.
[43] R.L. Pego, M. Weinstein, Convective linear stability of solitary waves for Boussinesq equations, Stud. Appl. Math. 99 (1997) 311–375.
[44] V.A. Dougalis, A. Durán, D.E. Mitsotakis, Numerical approximation of solitary waves of the Benjamin equation, Math. Comput. Simulation 127 (2016) 56–79.
[45] J. Alvarez, A. Duran, Petviashvili type methods for traveling wave computations: II. Acceleration with vector extrapolation methods, Math. Comput. Simulation 123 (2016) 19–36.
[46] E. Hairer, C. Lubich, G. Wanner, Geometric Numerical Integration, Structure-Preserving Algorithms for Ordinary Differential Equations, Springer-Verlag, New York, Heidelberg, Berlin, 2004.
[47] V.A. Dougalis, A. Durán, M.A. López-Marcos, D.E. Mitsotakis, A numerical study of the stability of solitary waves of the Bona-Smith family of Boussinesq systems, J. Nonlinear Sci. 17 (2007) 569–607.
[48] D.C. Antonopoulos, V.A. Dougalis, D.E. Mitsotakis, Numerical solution of Boussinesq systems of the Bona-Smith family, Appl. Numer. Math. 60 (2010) 314–336.